Dust Variability in the Middle East Recorded in the Elbrus Mt. Ice Core.

Dr. Stanislav Kutuzov (kutuzov@igras.ru)

Institute of Geography Russian Academy of Sciences, Moscow

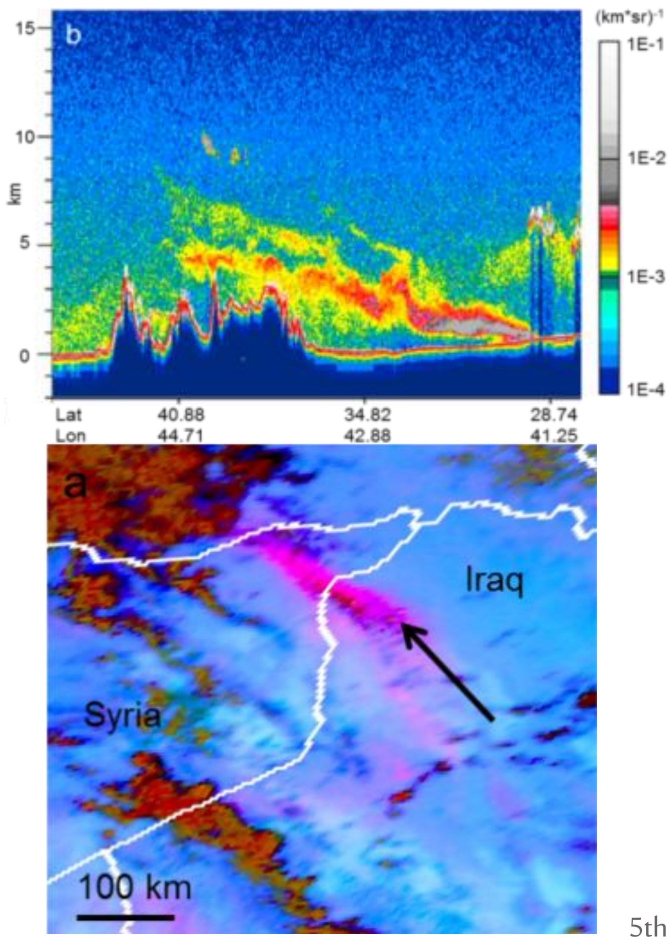

Over the past 50 years ice core records from polar (Greenland and Antarctic)and mountain regions were used to reconstruct the past environments for different time scales.

Greenland and Antarctic provided 800000 years record

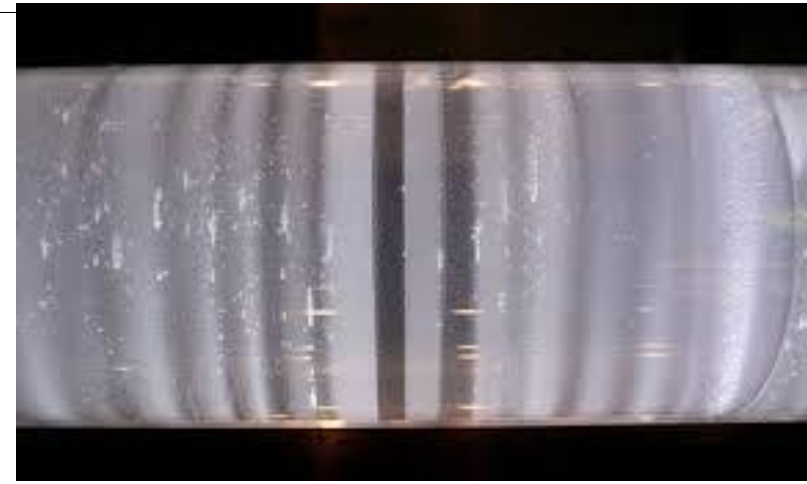

Ice cores are unique paleoenvironmental achieves

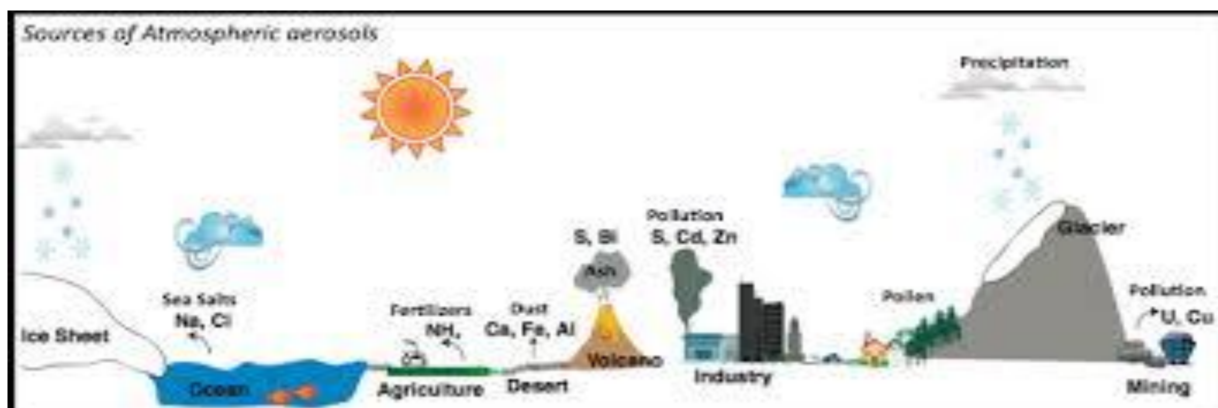

Dust records in Ice cores

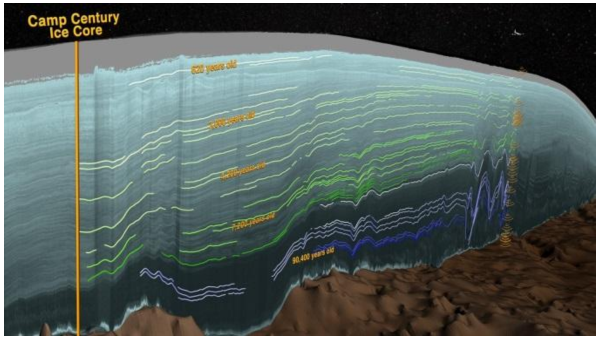

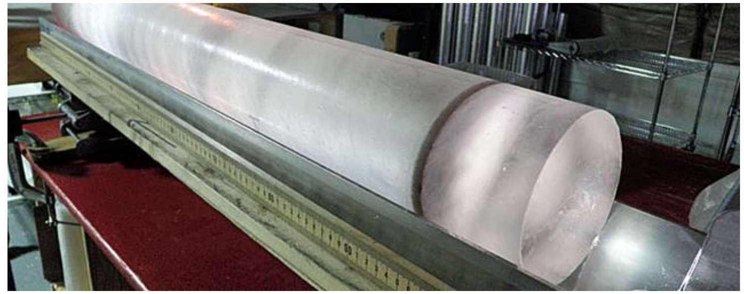

TABLE 1. Parameter Overview: List of Species and Measurement Methods of Mineral Dust Discussed in This Paper (Also Given Are the Respective Limits of Detection (LOD, Including Procedural Blanks) for Typical Applications)

acronym	species	method	LOD [μg/kg]
CC-mass	total water-insoluble particle mass (from particle volume)	Coulter counter	2
LPD-mass	total water-insoluble particle mass (from particle diameter)	laser-sensing particle detector	1
IC-Ca	soluble Ca^{2+}	ion chromatography	2
CFA-Ca	soluble Ca^{2+}	continuous flow analysis	0.1
nss-CFA-Ca*	soluble nonsea-salt Ca^{2+}	calculated [$(Na/Ca)_{sol,dust}$ = 0.91]	
ICPMS-digest-Al	total Al (full acid digestion)	ICP-MS	0.5
ICPMS-digest-Fe	total Fe (full acid digestion)	ICP-MS	0.2
ICPMS- HNO_3−Al	leachable Al (HNO_3-digestion at pH 1)	ICP-MS	0.1
ICPMS- HNO_3−Fe	leachable Fe (HNO_3-digestion at pH 1)	ICP-MS	0.03
ICPMS- HNO_3−V	leachable V (HNO_3-digestion at pH 1)	ICP-MS	0.001
PIXE-Al	water-insoluble, particulate dust Al	PIXE	0.8
PIXE-Ca	water-insoluble, particulate dust Ca	PIXE	0.2
PIXE-Fe	water-insoluble, particulate dust Fe	PIXE	0.1
PIXE-Si	water-insoluble, particulate dust Si	PIXE	0.7

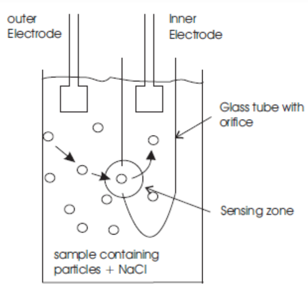

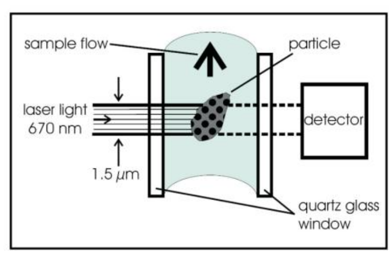

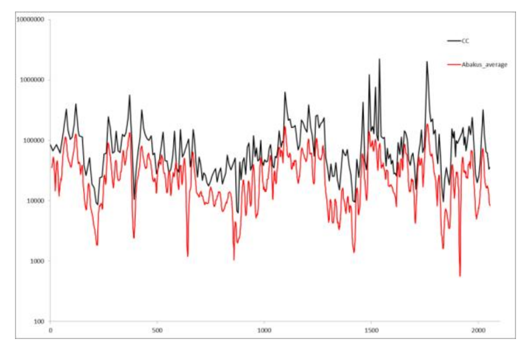

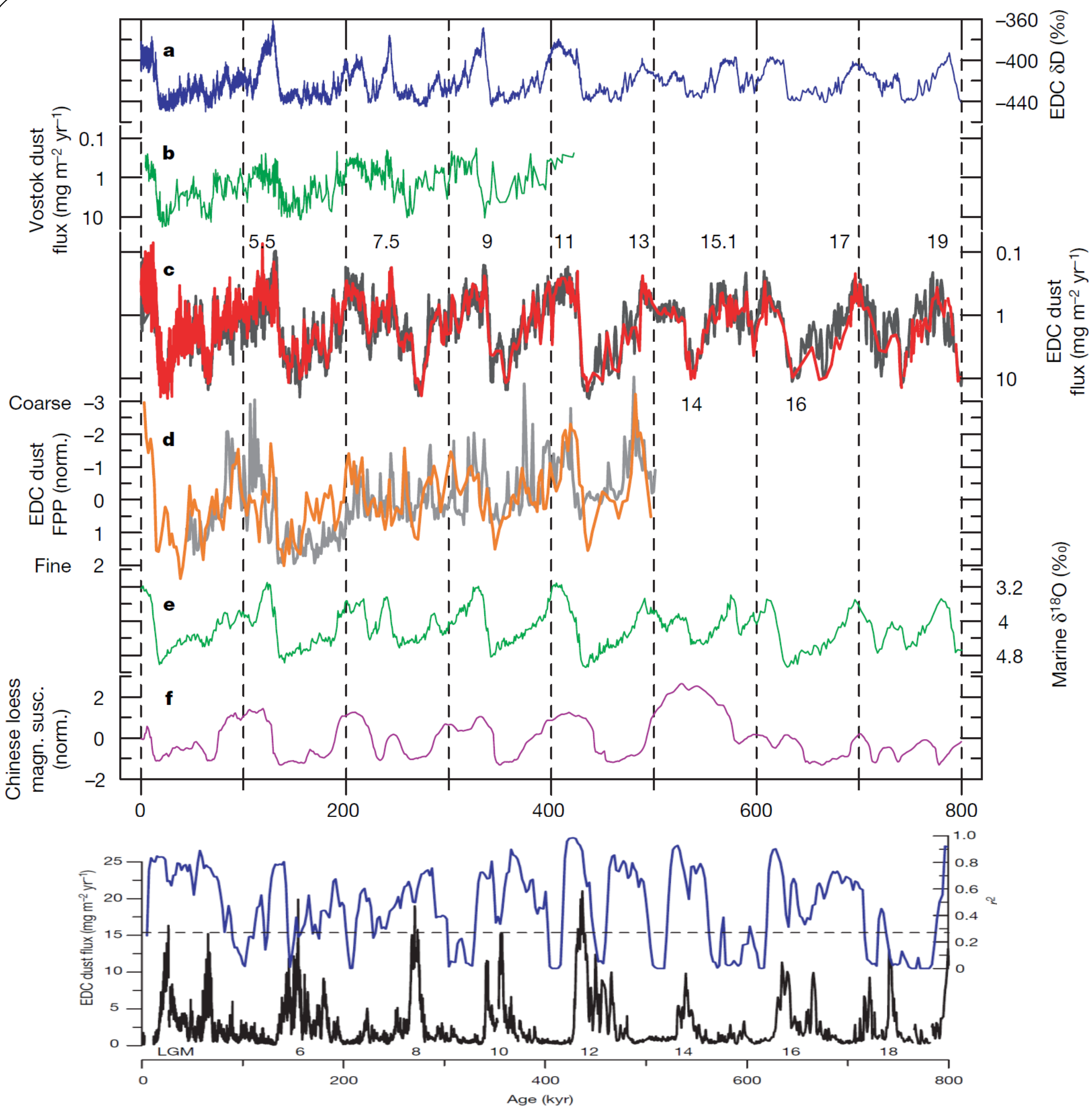

"The processes responsible for dust uptake and transport were not significantly altered from glacial to interglacial conditions. However, replenishment of dust supply, e.g. by glacial outwash, higher mean wind speeds, reduced precipitation, and vegetation can explain a largely increased glacial source strength in southern South America.

Together with the larger atmospheric residence time connected to lower precipitation en route, this may explain a large part of the **25 times higher** dust fluxes in Antarctica during glacials." (Lambert et al., 2012)

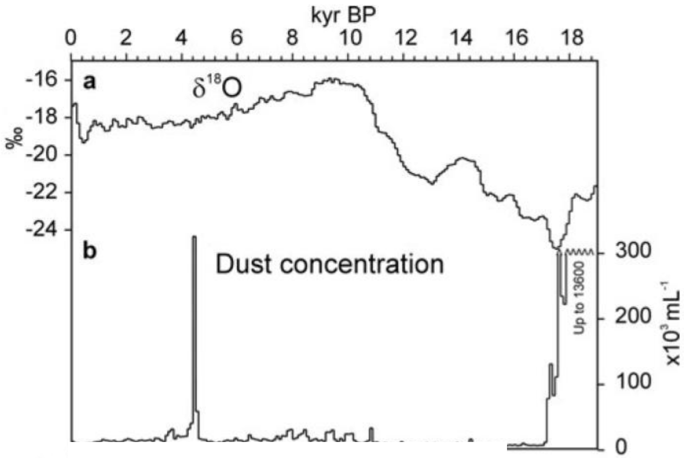

An Andean ice-core record of a Middle Holocene mega-drought in North Africa and Asia

Mary E. DAVIS, Lonnie G. THOMPSON 2006

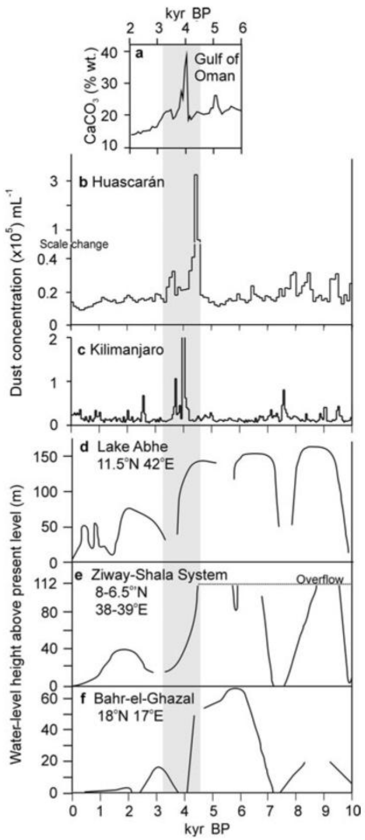

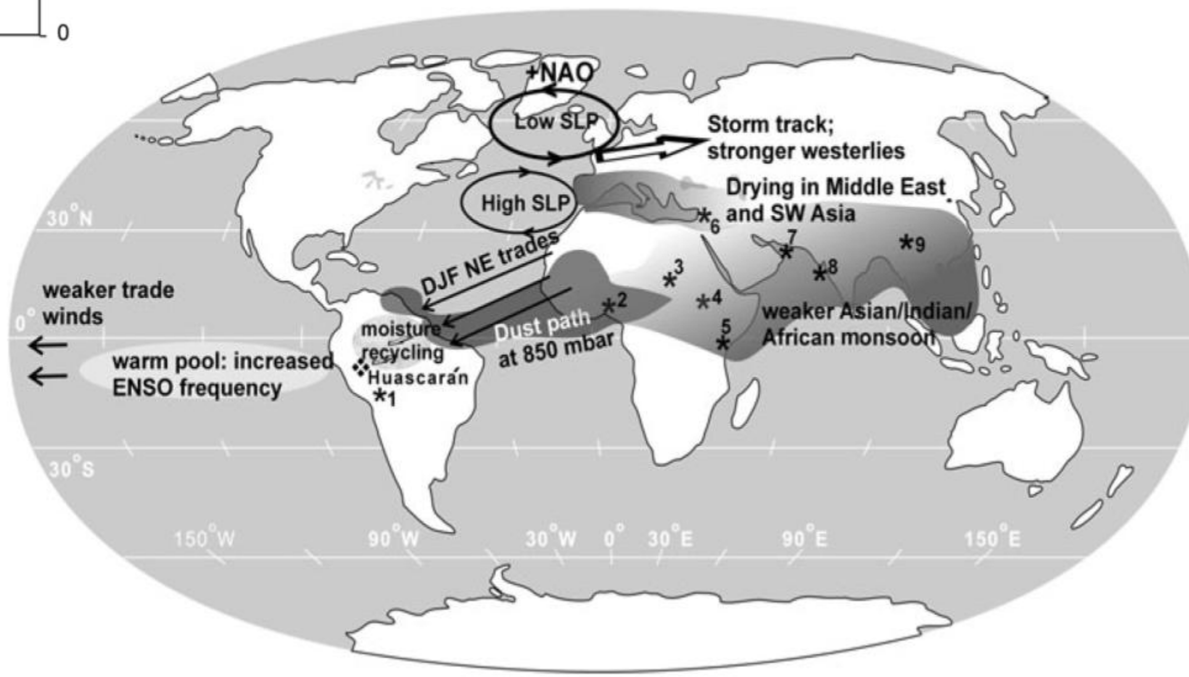

20th Century Dust Lows and the Weakening of the Westerly Winds over the Tibetan Plateau (Grigholm et al., 2015)

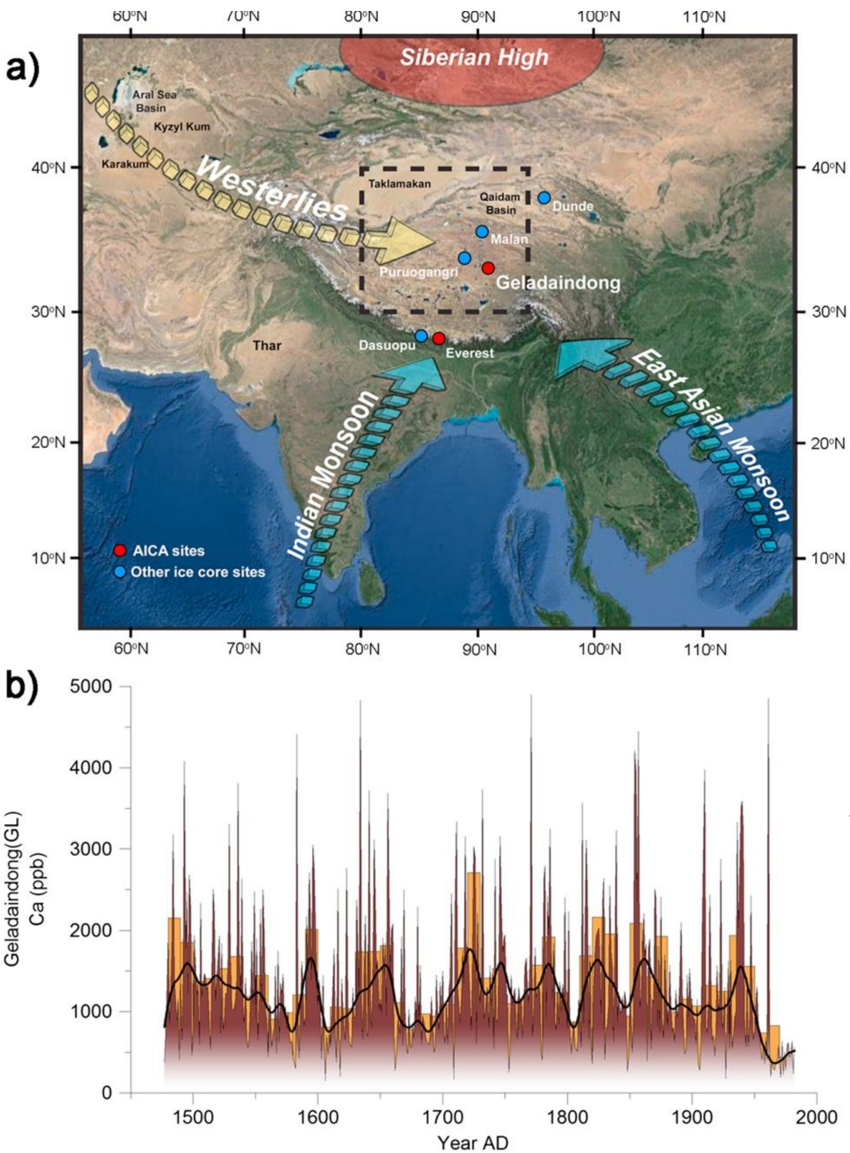

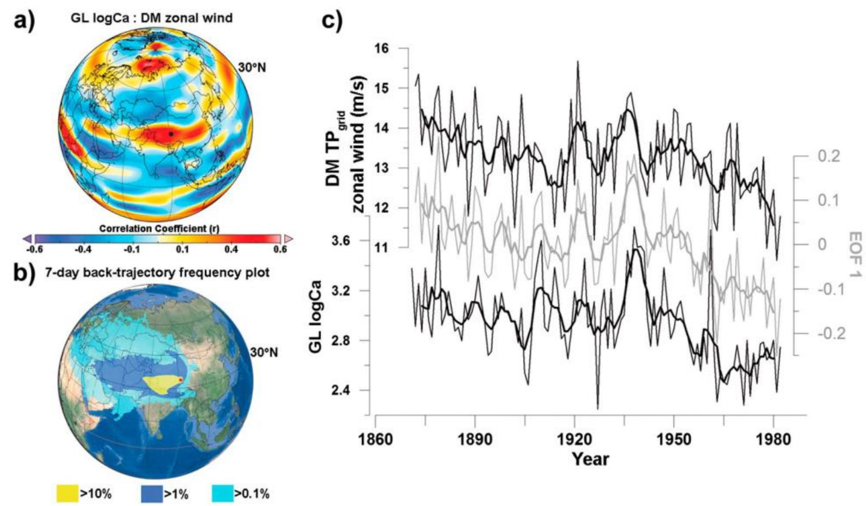

Decline in Ca concentrations correspond with regional trends in reduced zonal wind strengths.

Twentieth century declines in zonal wind velocities, and the subsequent declines in dust transport over the TP, are likely the result of increased temperatures lowering meridional pressure gradients (i.e., weakening the SH) over large portions of northern Asia.

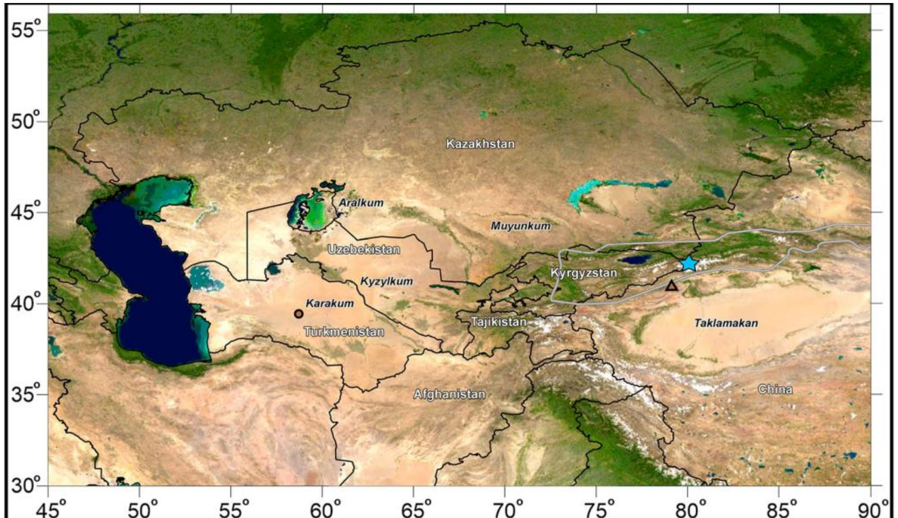

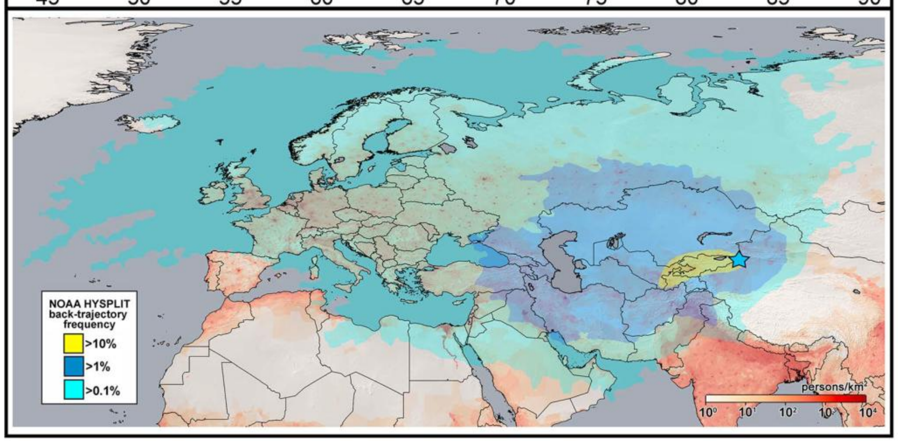

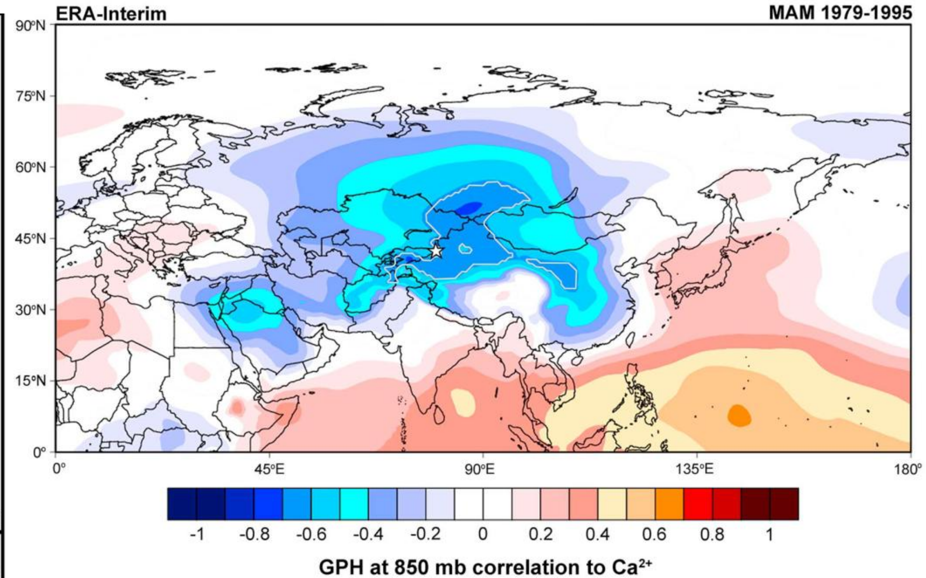

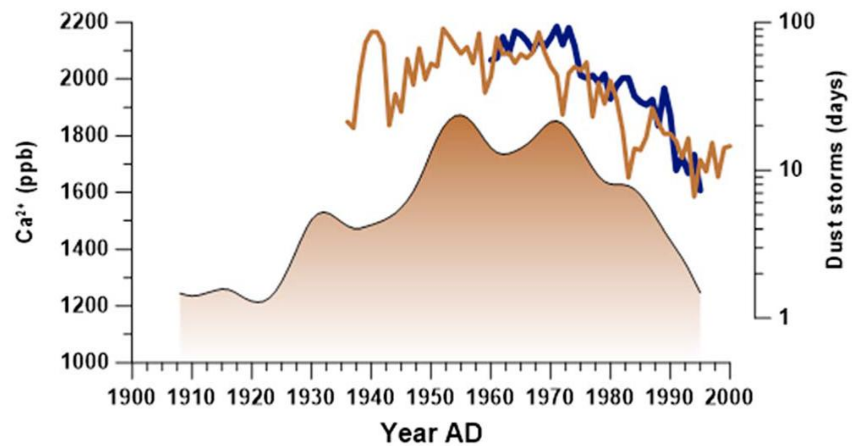

A twentieth century major soluble ion record of dust and anthropogenic pollutants from Inilchek Glacier, Tien Shan

B. Grigholm[1], P. A. Mayewski[1], V. Aizen[2], K. Kreutz[1], E. Aizen[2], S. Kang[3,4], K. A. Maasch[1], and S. B. Sneed[1]

Figure 6. Comparison between Inilchek Ca^{2+} concentrations (brown gradient-robust spline) (tension 0.01) and annual dust storm days at Kalpin, Xinjiang, China (blue), and Erbent, Turkmenistan (brown) [*Xiao et al.*, 2008; *Indoitu et al.*, 2012].

The impact of Saharan dust and black carbon on albedo and long-term mass balance of an Alpine glacier

J. Gabbi[1], M. Huss[1,2], A. Bauder[1], F. Cao[3,4], and M. Schwikowski[3]

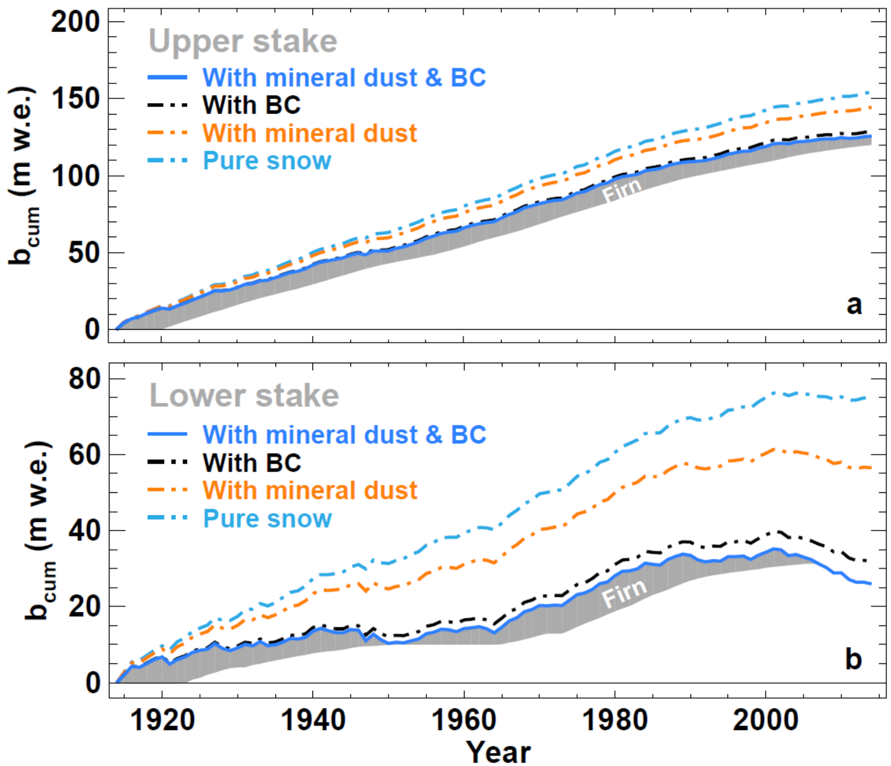

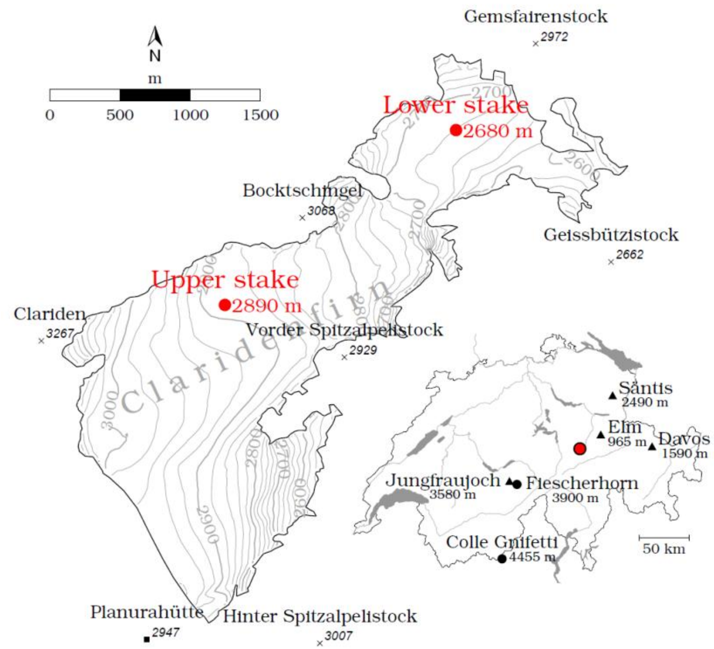

Due to the combined effect of BC and Saharan dust, annual ablation on Claridenfirn was increased by 15–19% on average over 1914–2014 compared to pure snow conditions.

Mahowald et al 2010 Observed 20th century desert dust variability: impact on climate and biogeochemistry

Dust sources strength?

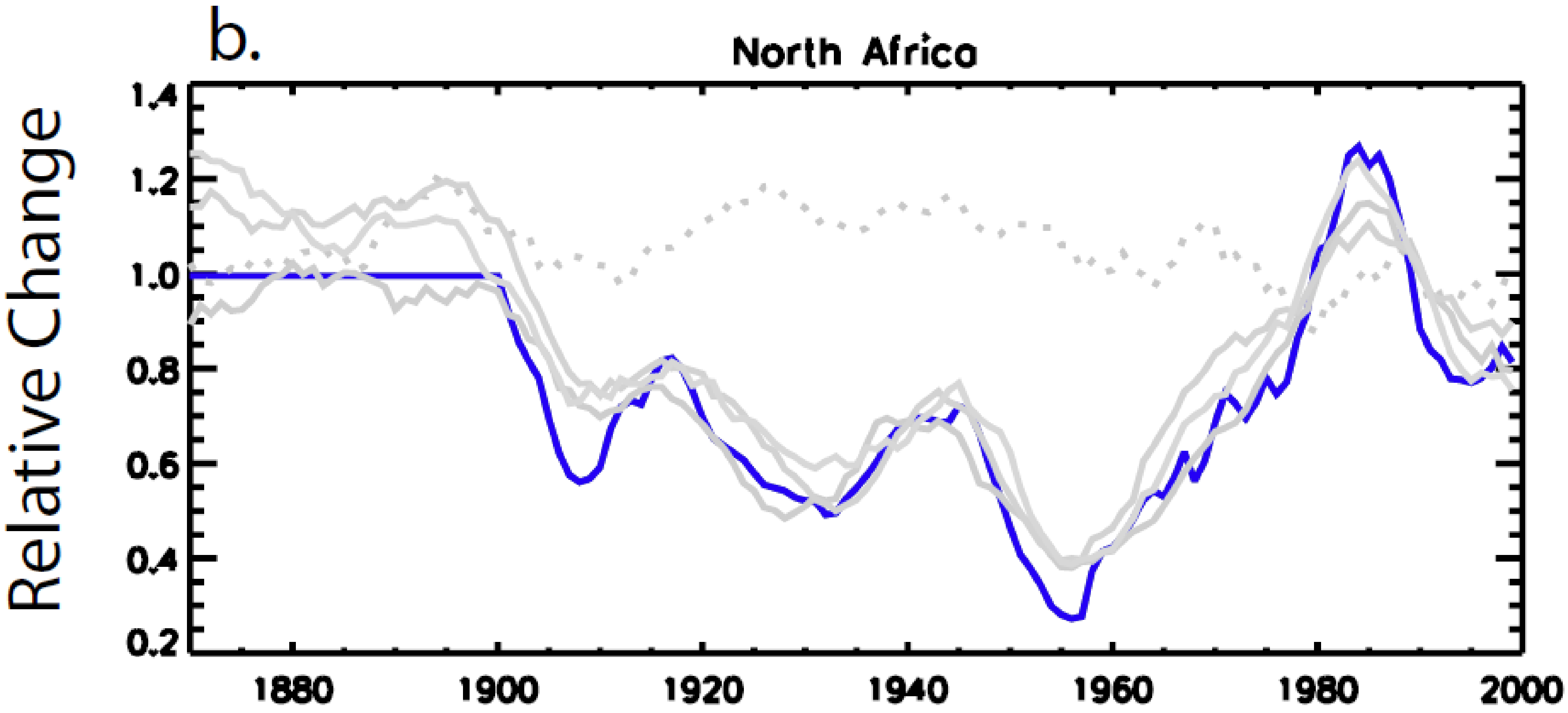

Motivation

- Understanding climate change, regional environmental patterns, and predicting future impacts are currently some of the most important scientific challenges.
- Ice cores from low and mid-latitude high mountain glaciers provide a valuable information about past atmospheric conditions in areas with long human histories.
- Conditions near the top of Mt. Elbrus suggest the possibility of a reasonably long climatic record in an ice core not affected by meltwater infiltration and relatively high accumulation on the western plateau assures high temporal resolu[redacted]

The Caucasus Mountains located between the Black and the Caspian Seas in proximity to the arid regions.

Region is affected by desert dust deposition but has not been studied in this respect

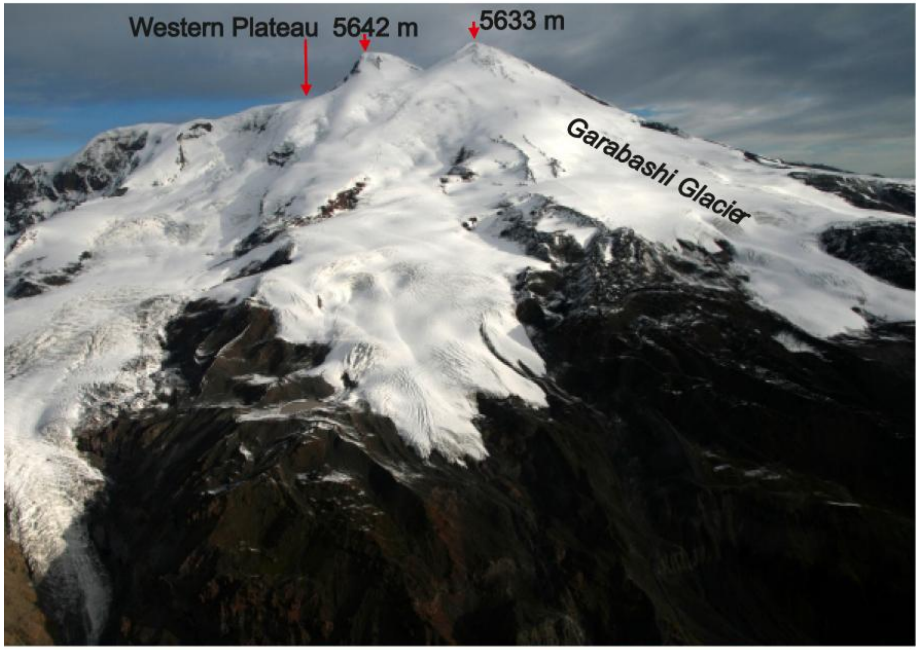

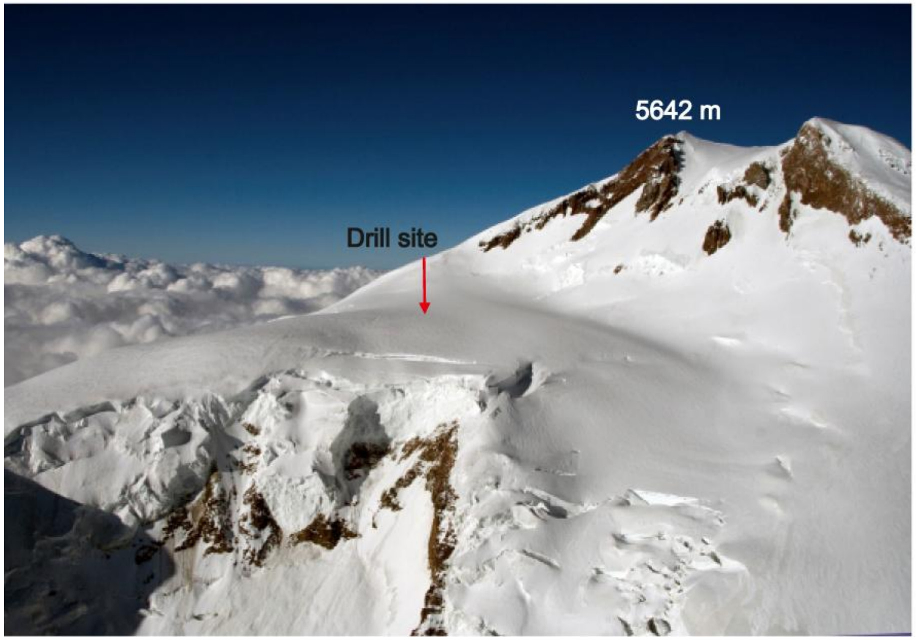

The Mt. Elbrus, the highest summit of the Caucasus (5642 m asl)

The Western Plateau of Mt. Elbrus is located at the western slope of Elbrus at 5115 m. The plateau restricted on south and south-east by two lava ridges, and by vertical wall of Mt. Elbrus on the east.

182 m ice core was drilled in 2009.

This is the first ice core from this region, representing practically un-disturbed by seasonal melting paleoclimate record, with the possibility to analyze the intra-seasonal climate proxies variability with high temporal resolution.

(Mikhalenko et al., 2015)

ELBRUS Ice core records

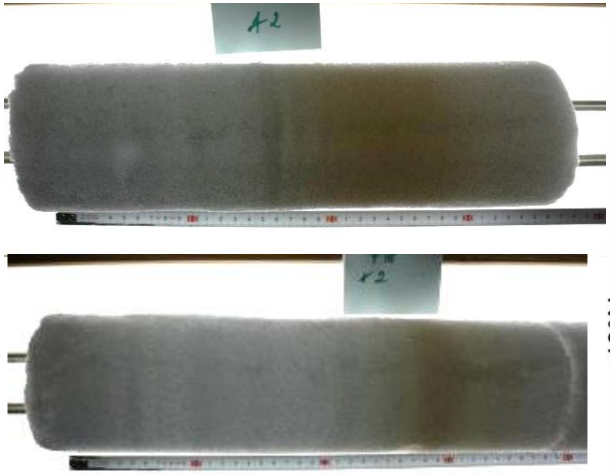

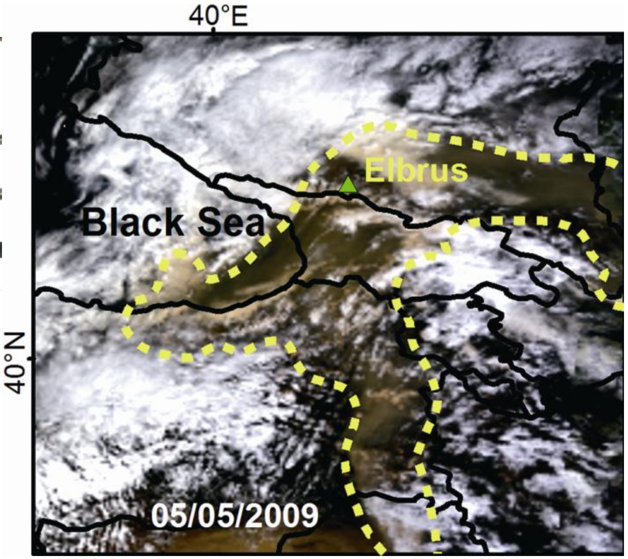

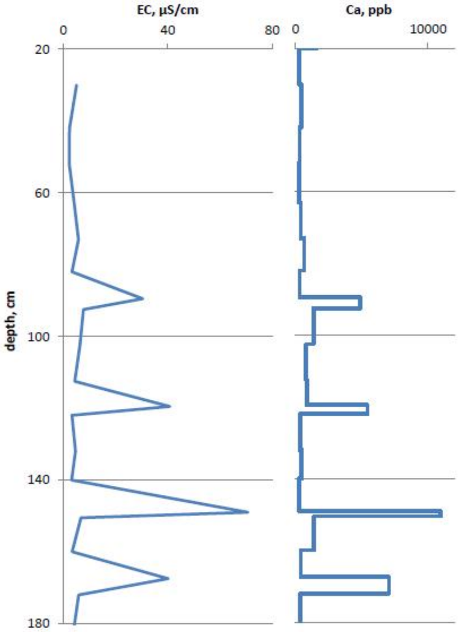

Shahgedanova et al. 2013

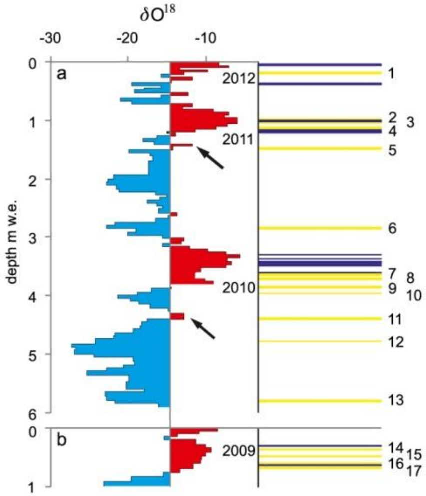

Kutuzov et al., 2013

Remote sensing: SEVIRI; MODIS Deep Blue and SEVIRI AOD; CALIOP, reanalysis, trajectory models: HYSPLIT,ADC

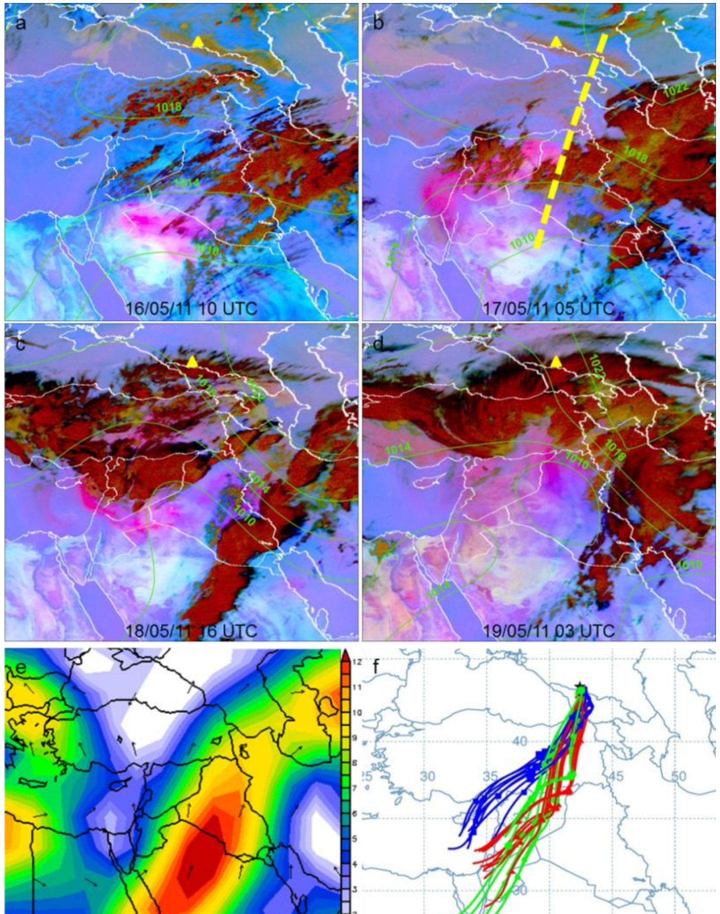

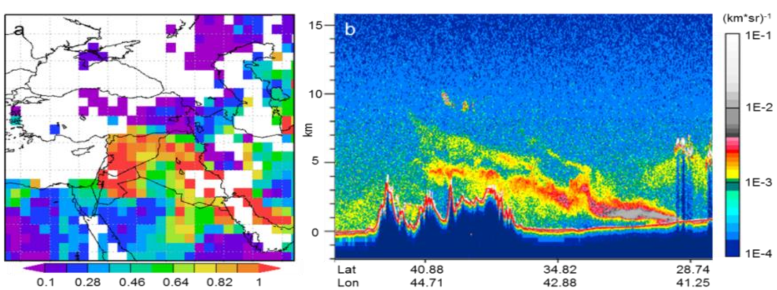

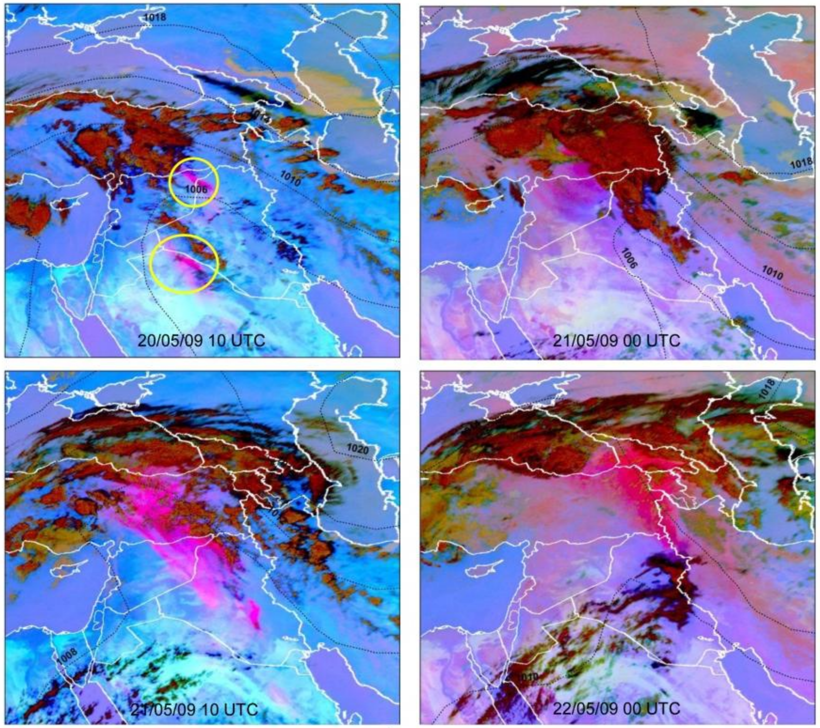

Dust transport from the Middle East is controlled by the development of low pressure systems over the Middle East-Turkey-Black Sea region and high pressure centred over or extending towards the Caspian Sea enabling the development of southerly or south-easterly flow towards the Caucasus.

Dust transport from Sahara was associated with deep depressions and strong air flow and resulted in high dust loads

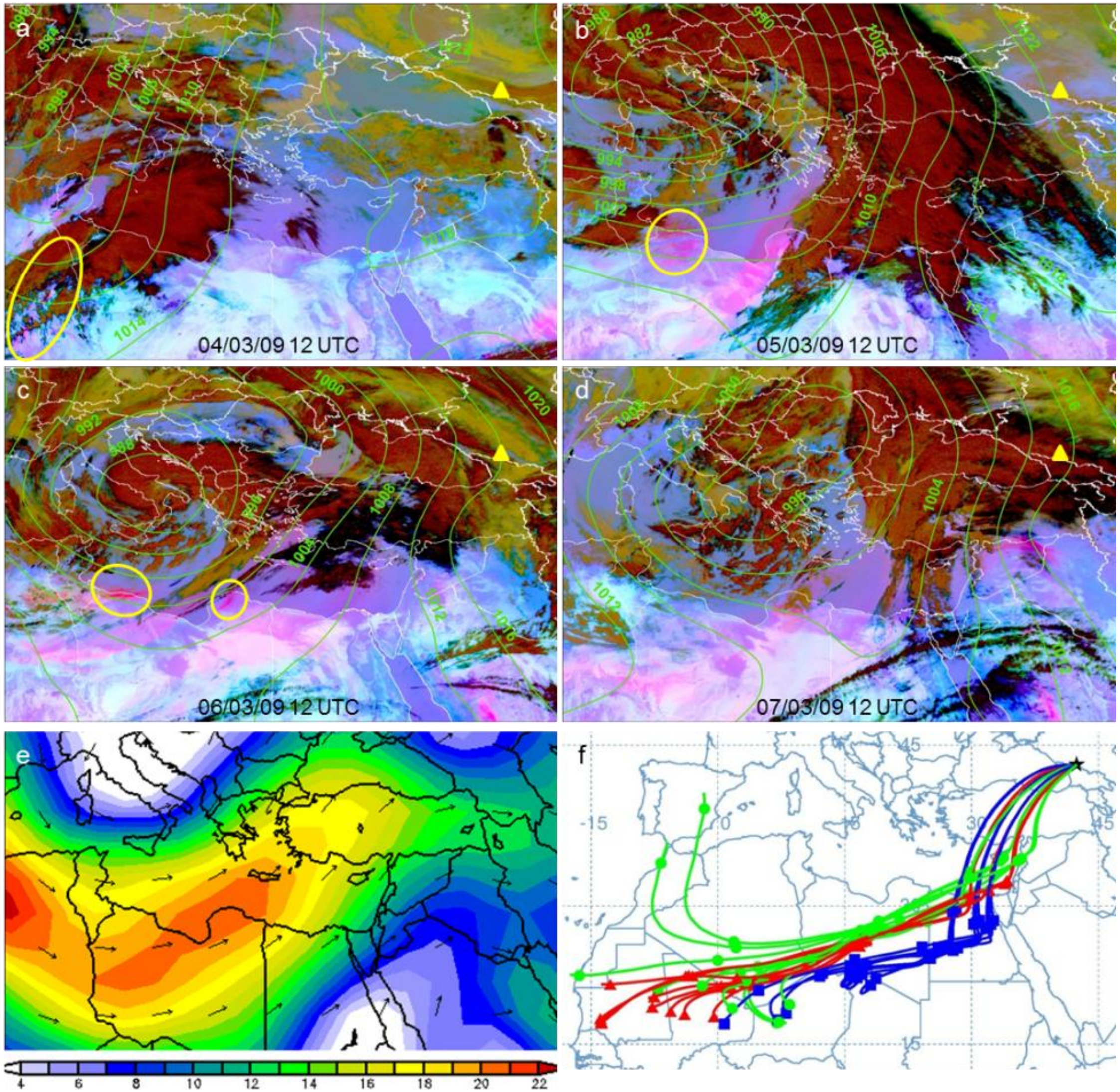

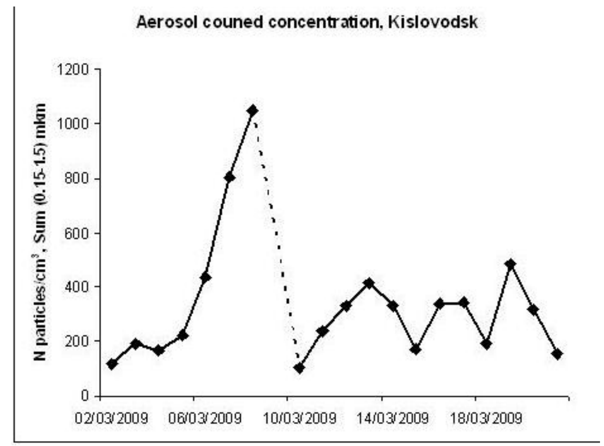

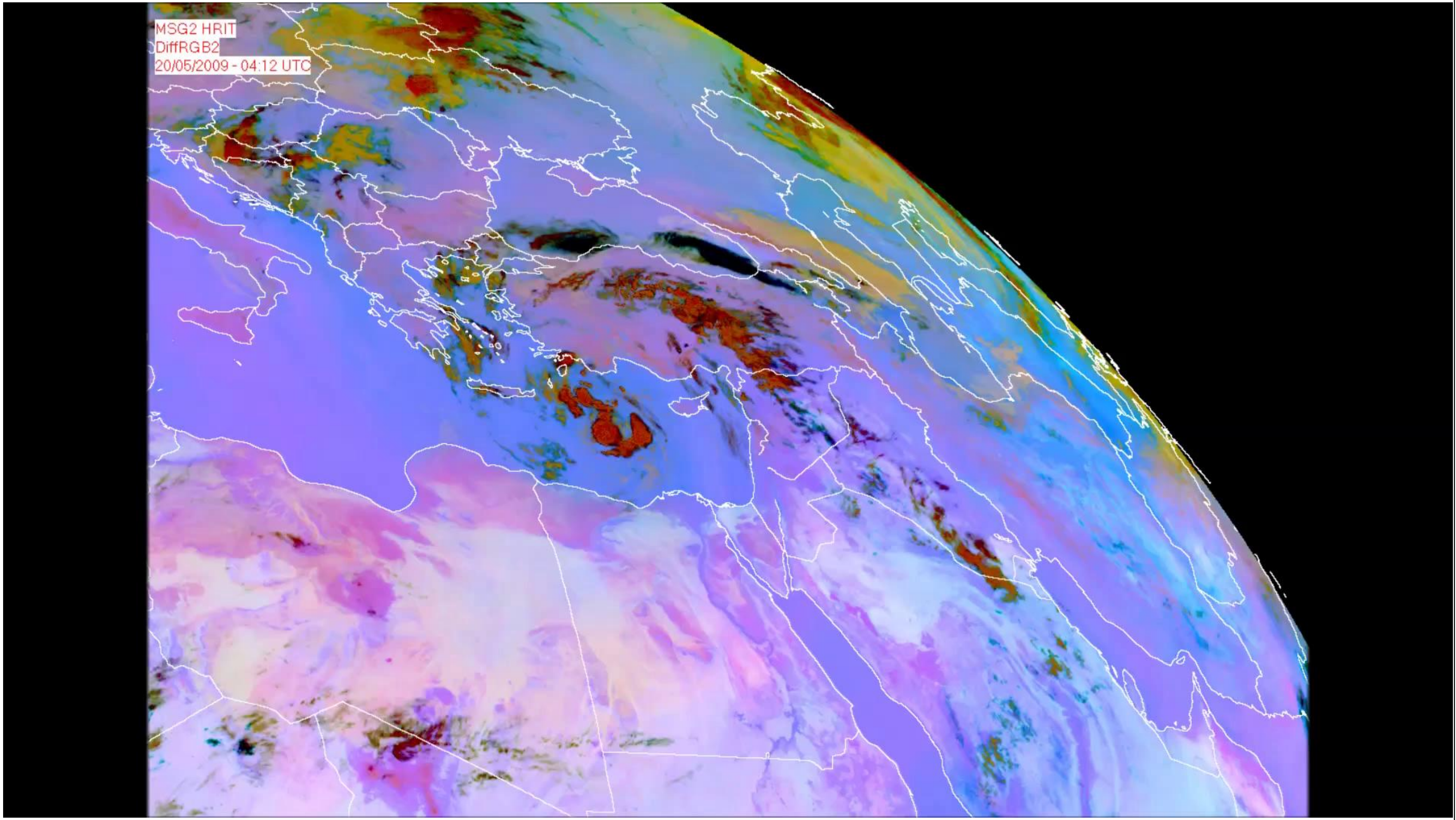
MSG2 HRIT
DiffRGB2
20/05/2009 - 04:12 UTC

Dust sources

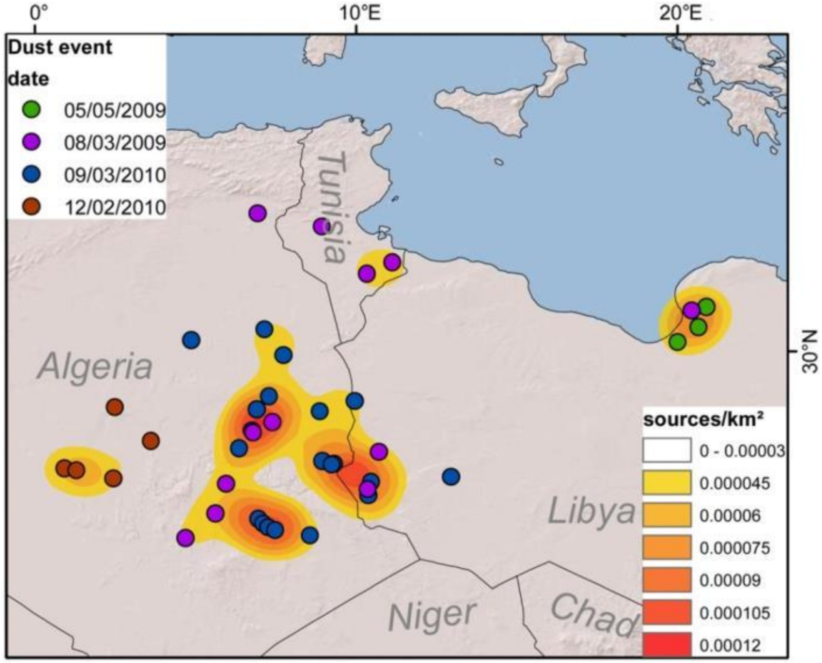

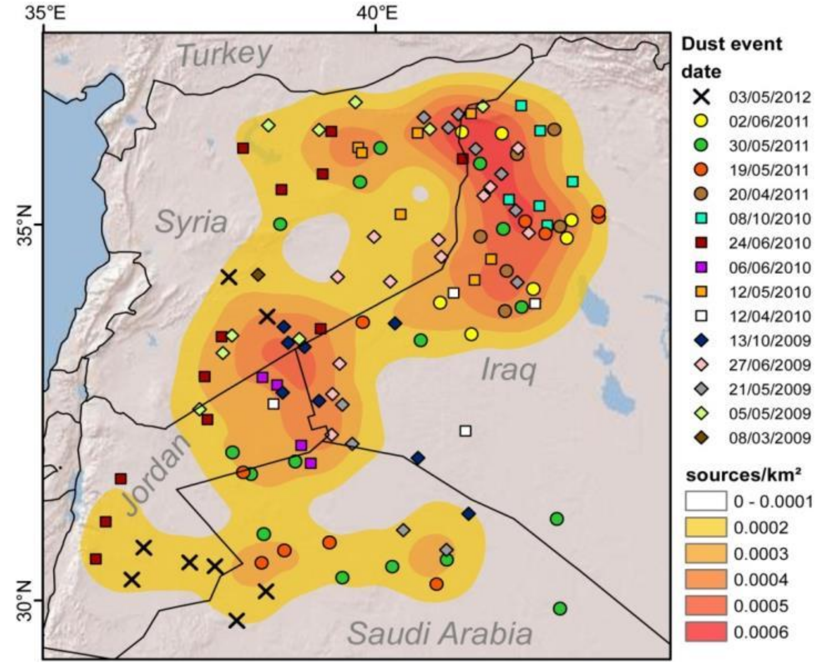

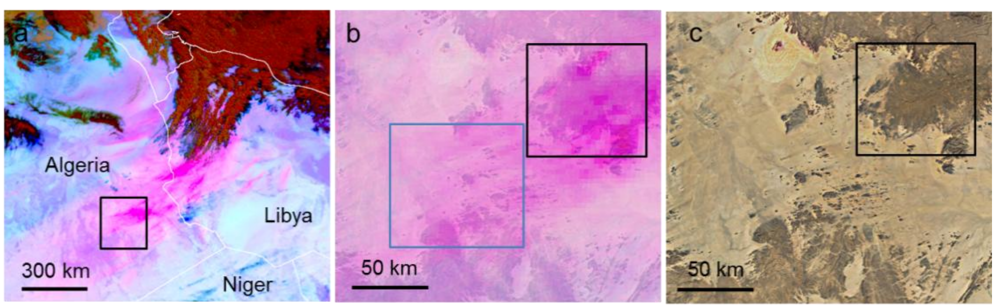

Saharan sources: extensive natural sources endorheic water systems (wadis opening to alluvial fans or chotts.

Eastern and Central Algeria, the Djebel Akhdar in Libya and Tunisia

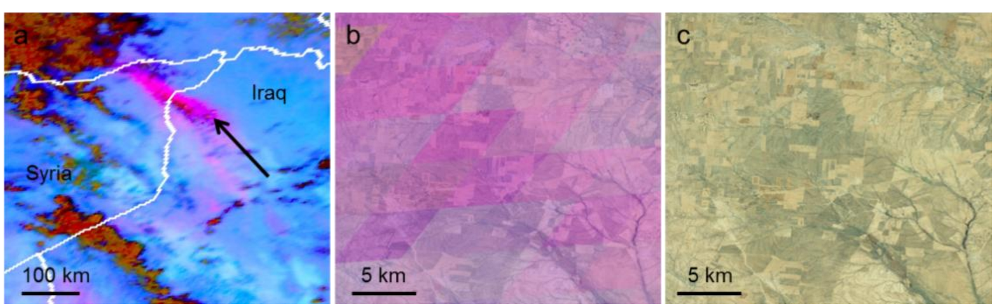

Middle East sources multiple small-scale sources both natural (dry river beds and lakes) and anthropogenic, predominantly agricultural sources.

Northern Mesopotamia and the Syrian Desert

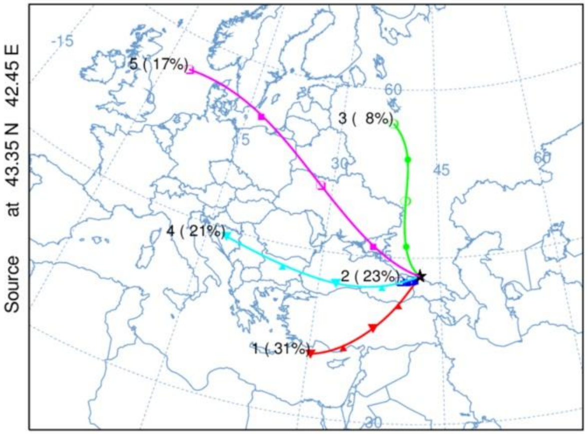

Cluster means - Elb_2013
979 backward trajectories
CDC1 Meteorological Data

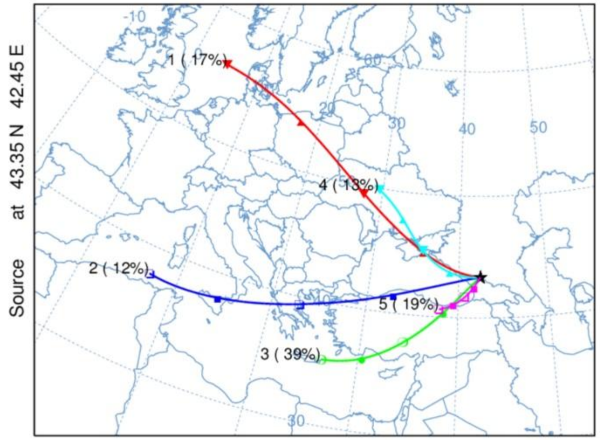

Cluster means - Elb_march-october2008
980 backward trajectories
CDC1 Meteorological Data

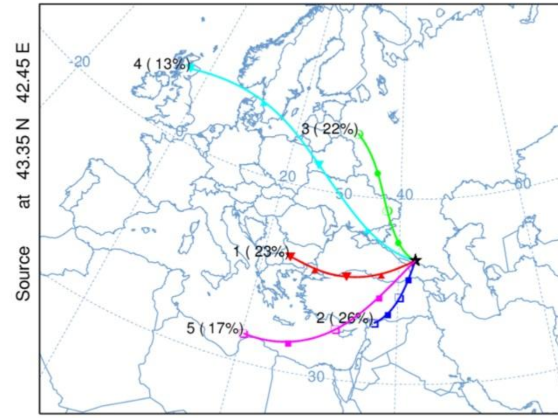

Cluster means - Elb_march-october2011
980 backward trajectories
CDC1 Meteorological Data

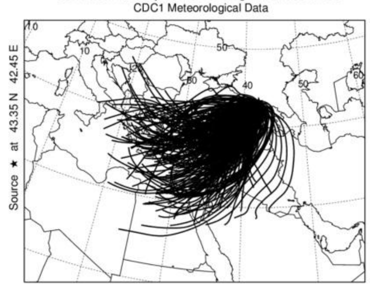

Cluster 1 of 5 - Elb_2013
304 backward trajectories ending at various times
CDC1 Meteorological Data

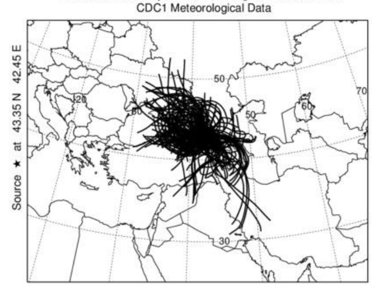

Cluster 2 of 5 - Elb_2013
222 backward trajectories ending at various times
CDC1 Meteorological Data

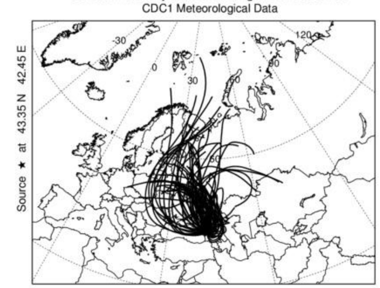

Cluster 3 of 5 - Elb_2013
80 backward trajectories ending at various times
CDC1 Meteorological Data

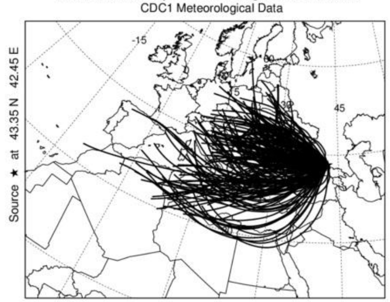

Cluster 4 of 5 - Elb_2013
206 backward trajectories ending at various times
CDC1 Meteorological Data

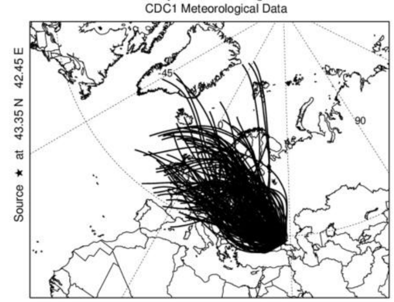

Cluster 5 of 5 - Elb_2013
167 backward trajectories ending at various times
CDC1 Meteorological Data

DUST flux

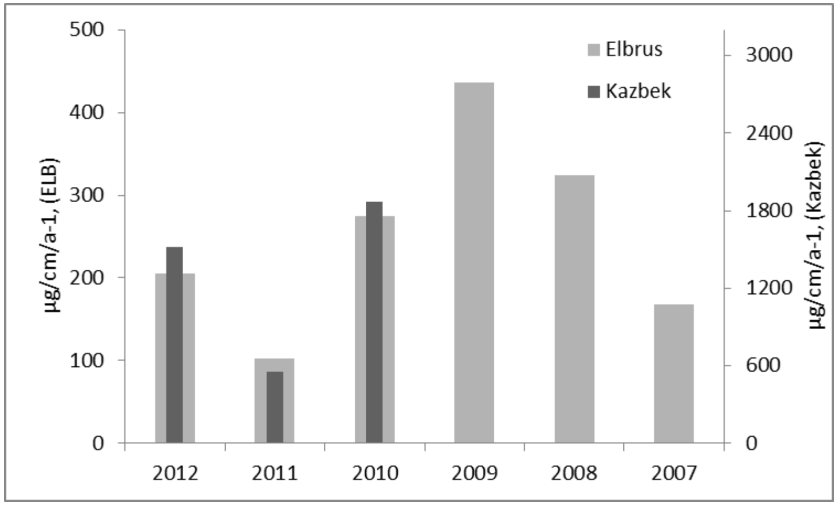

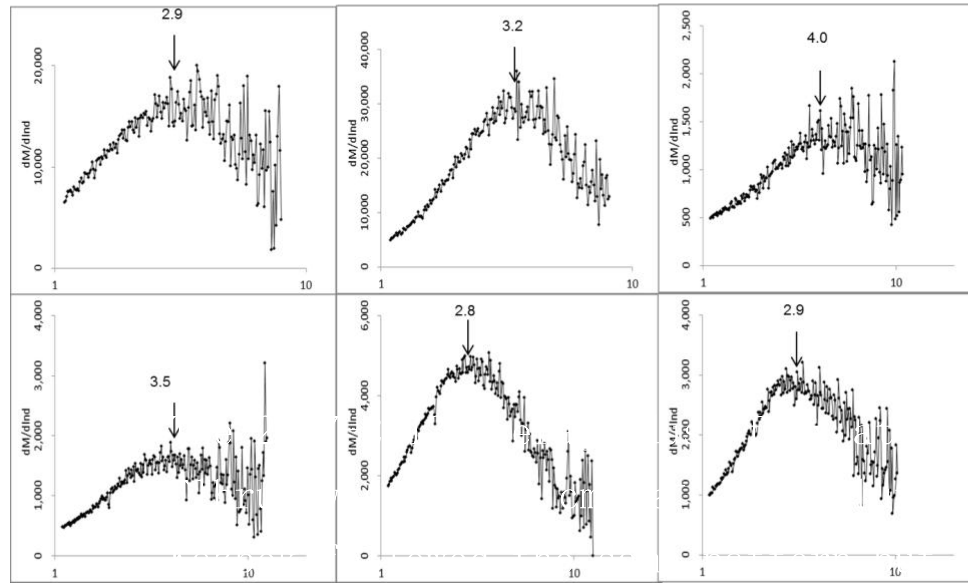

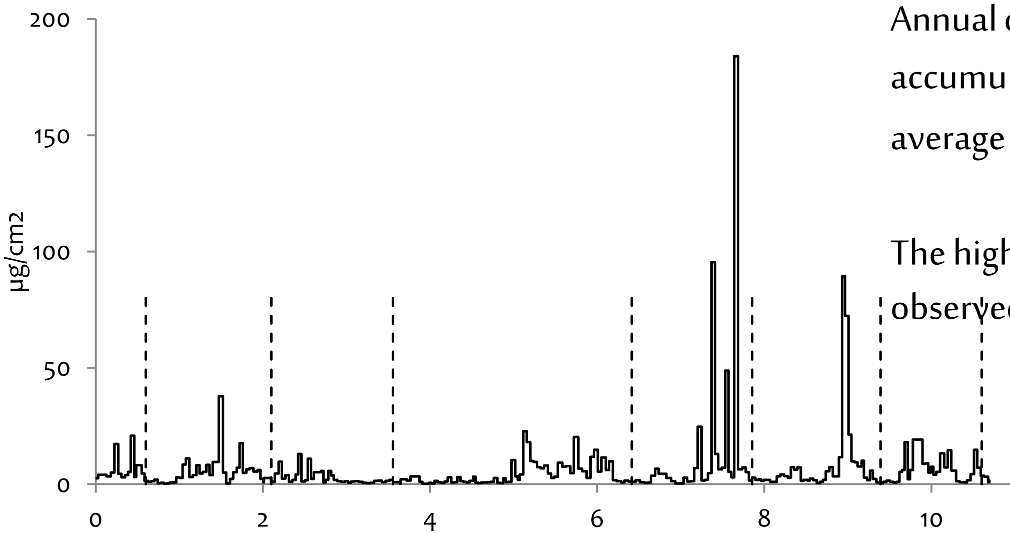

Annual dust fluxes were calculated for 6 years using accumulation data and average annual C_m. The 2007-2013 average dust flux was 252 $\mu g\ cm^{-2}\ a^{-1}$.

The highest dust fluxes of 437 and 324 $\mu g\ cm^{-2}\ a^{-1}$ were observed in 2009 and 2008 respectively.

Mineralogy

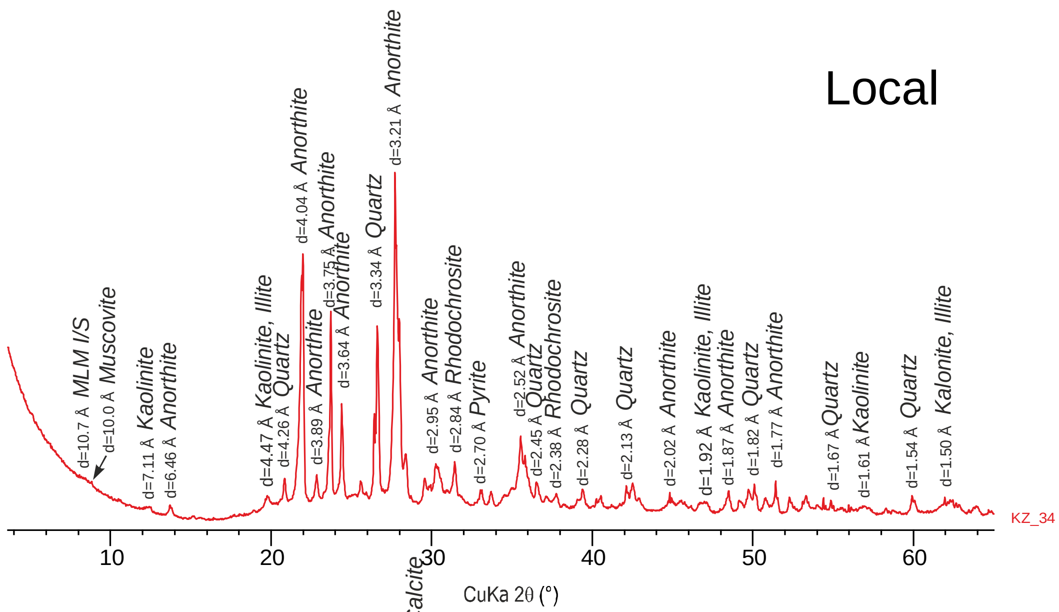

Local
d=10.7 Å MLM I/S
d=10.0 Å Muscovite
d=7.11 Å Kaolinite
d=6.46 Å Anorthite
d=4.47 Å Kaolinite, Illite
d=4.26 Å Quartz
d=4.04 Å Anorthite
d=3.89 Å Anorthite
d=3.75 Å Anorthite
d=3.64 Å Anorthite
d=3.34 Å Quartz
d=3.21 Å Anorthite
d=2.95 Å Anorthite
d=2.84 Å Rhodochrosite
d=2.70 Å Pyrite
d=2.52 Å Anorthite
d=2.45 Å Quartz
d=2.38 Å Rhodochrosite
d=2.28 Å Quartz
d=2.13 Å Quartz
d=2.02 Å Anorthite
d=1.92 Å Kaolinite, Illite
d=1.87 Å Anorthite
d=1.82 Å Quartz
d=1.77 Å Anorthite
d=1.67 Å Quartz
d=1.61 Å Kaolinite
d=1.54 Å Quartz
d=1.50 Å Kalonite, Illite
KZ_34
10
20
30
40
50
60
CuKa 2θ (°)

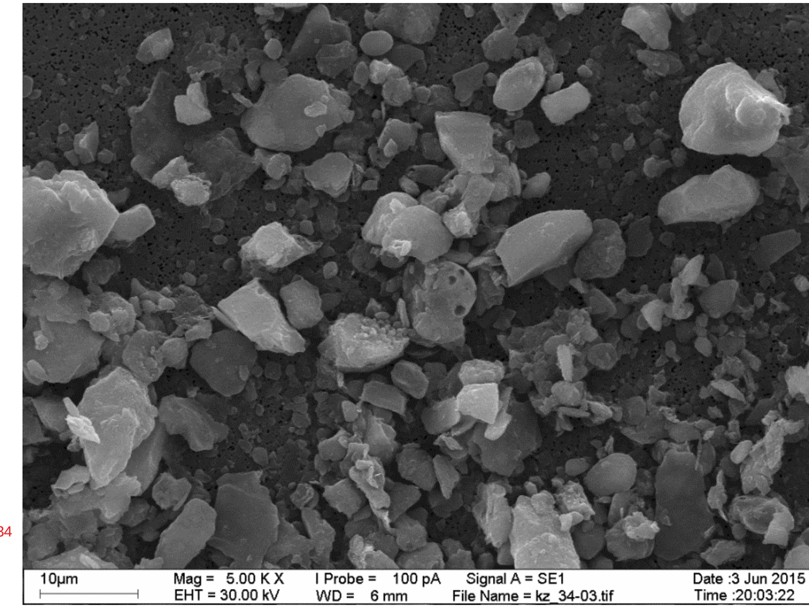

10μm
Mag = 5.00 K X
EHT = 30.00 kV
I Probe = 100 pA
WD = 6 mm
Signal A = SE1
File Name = kz_34-03.tif
Date :3 Jun 2015
Time :20:03:22

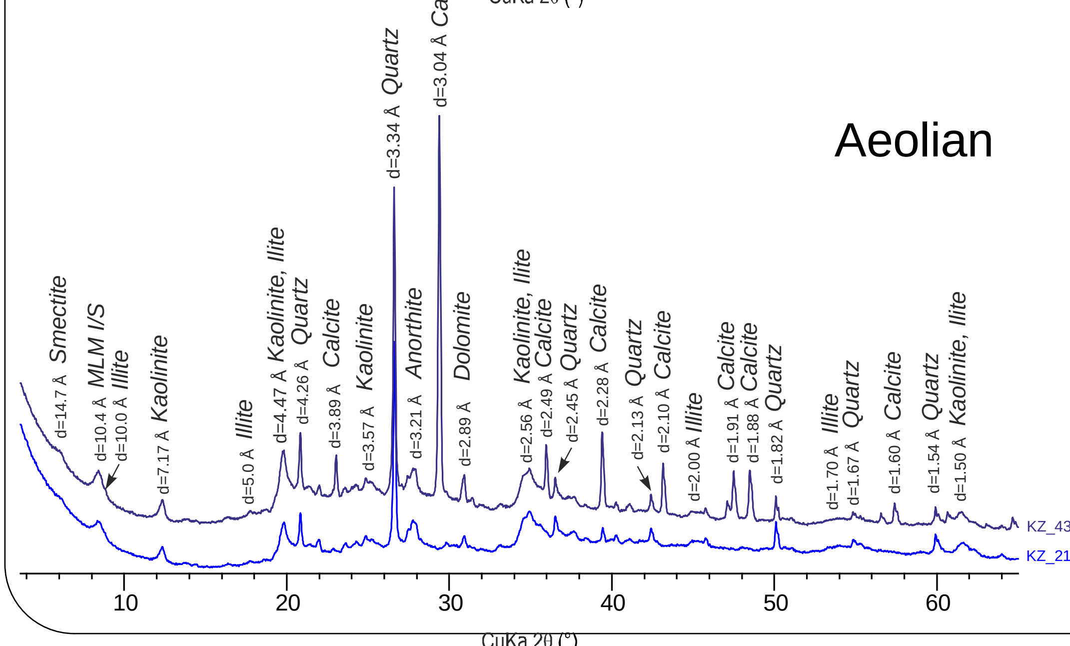

Aeolian
d=14.7 Å Smectite
d=10.4 Å MLM I/S
d=10.0 Å Illite
d=7.17 Å Kaolinite
d=5.0 Å Illite
d=4.47 Å Kaolinite, Ilite
d=4.26 Å Quartz
d=3.89 Å Calcite
d=3.57 Å Kaolinite
d=3.34 Å Quartz
d=3.21 Å Anorthite
d=3.04 Å Calcite
d=2.89 Å Dolomite
d=2.56 Å Kaolinite, Ilite
d=2.49 Å Calcite
d=2.45 Å Quartz
d=2.28 Å Calcite
d=2.13 Å Quartz
d=2.10 Å Calcite
d=2.00 Å Illite
d=1.91 Å Calcite
d=1.88 Å Calcite
d=1.82 Å Quartz
d=1.70 Å Illite
d=1.67 Å Quartz
d=1.60 Å Calcite
d=1.54 Å Quartz
d=1.50 Å Kalonite, Illite
KZ_43
KZ_21
10
20
30
40
50
60
CuKa 2θ (°)

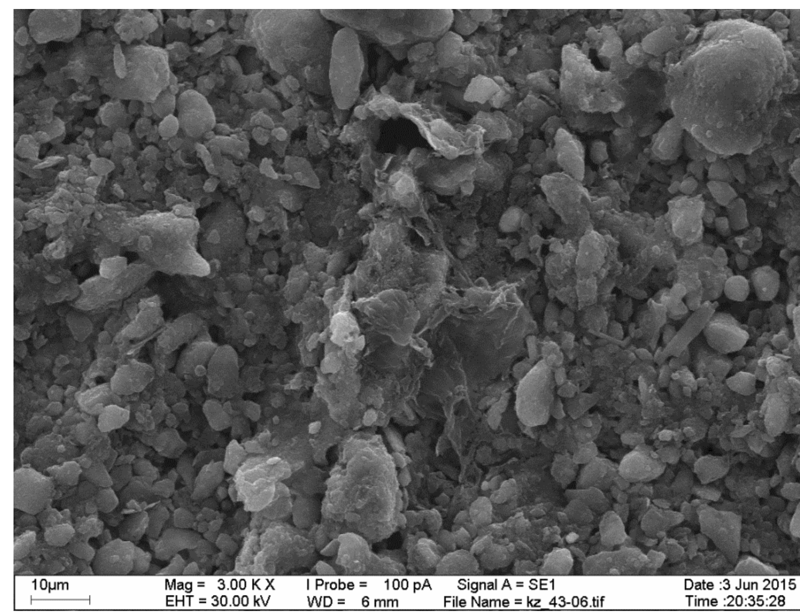

10μm
Mag = 3.00 K X
EHT = 30.00 kV
I Probe = 100 pA
WD = 6 mm
Signal A = SE1
File Name = kz_43-06.tif
Date :3 Jun 2015
Time :20:35:28

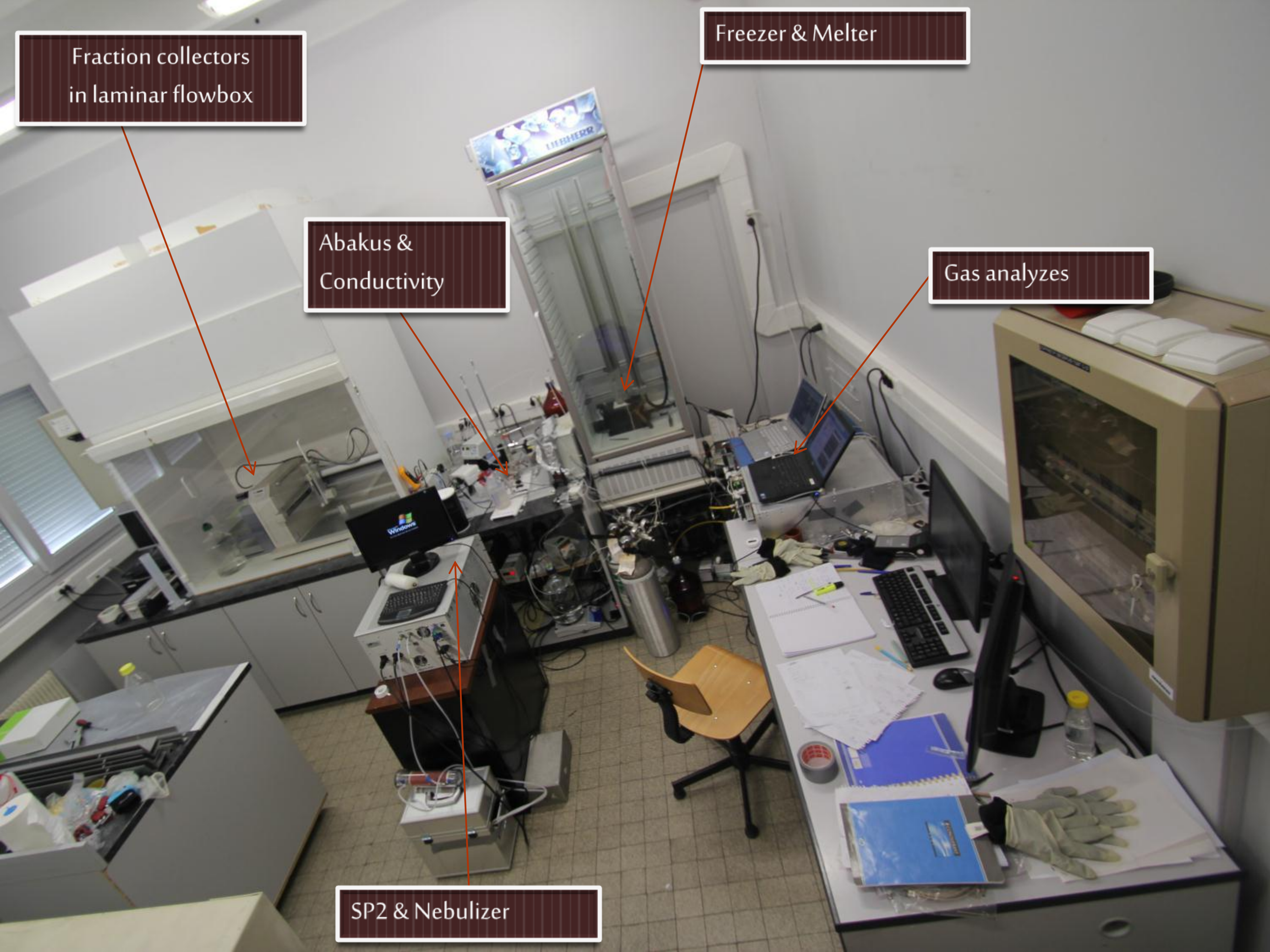
Fraction collectors in laminar flowbox
Freezer & Melter
Abakus & Conductivity
Gas analyzes
SP2 & Nebulizer

Ice core dating

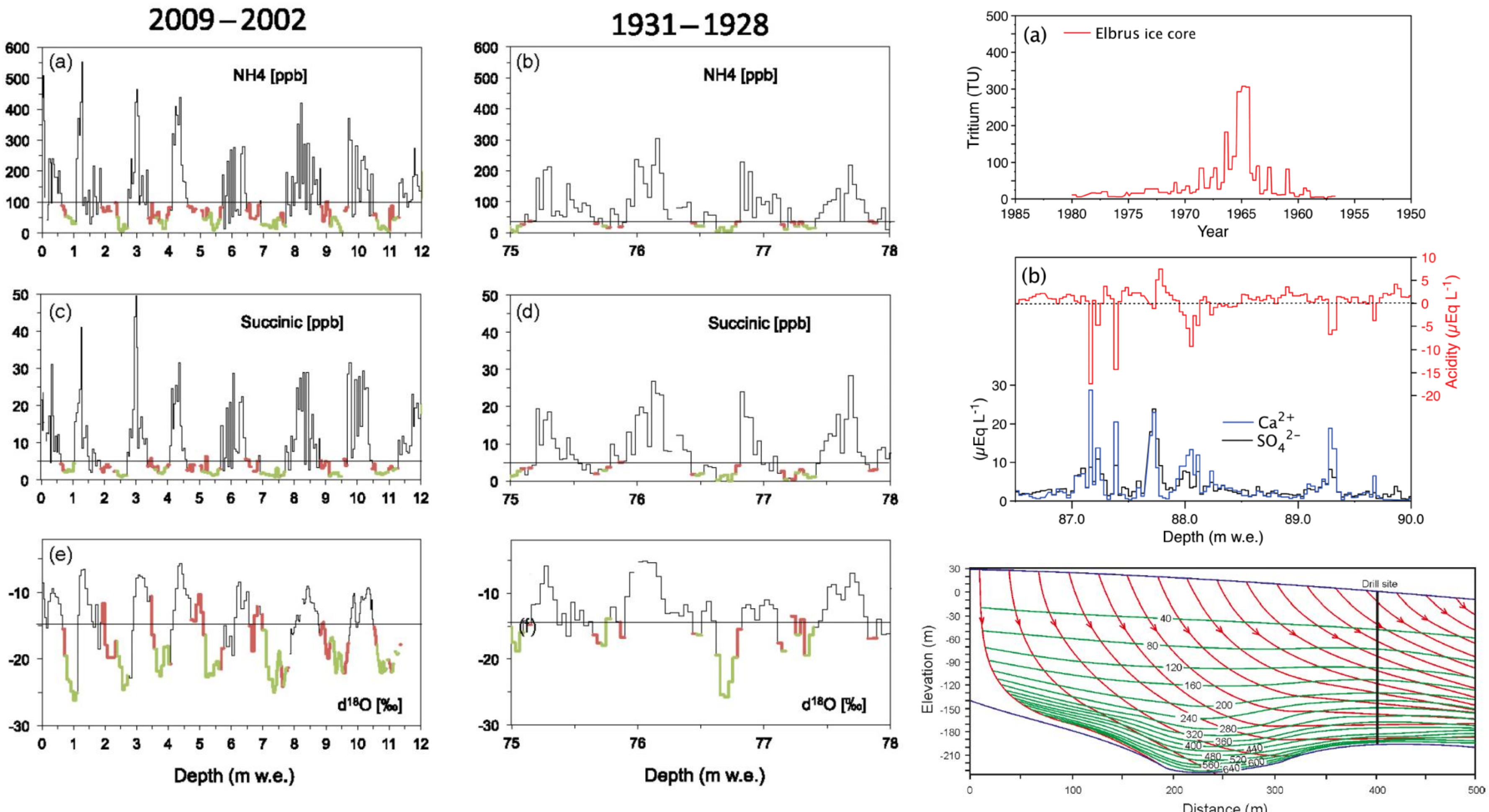

Annual layers were differentiated on the basis of seasonal oscillations of NH4 , succinic acid, and δ18O.

Annual layer counting was confirmed by the well-known reference horizons of the AD1963 nuclear tests and the AD1912 Katmai volcanic eruption.

Ice flow models show that the basal ice age at the maximum glacier depth of 255m is more than 600 years BP

Mikhalenko et al., 2015

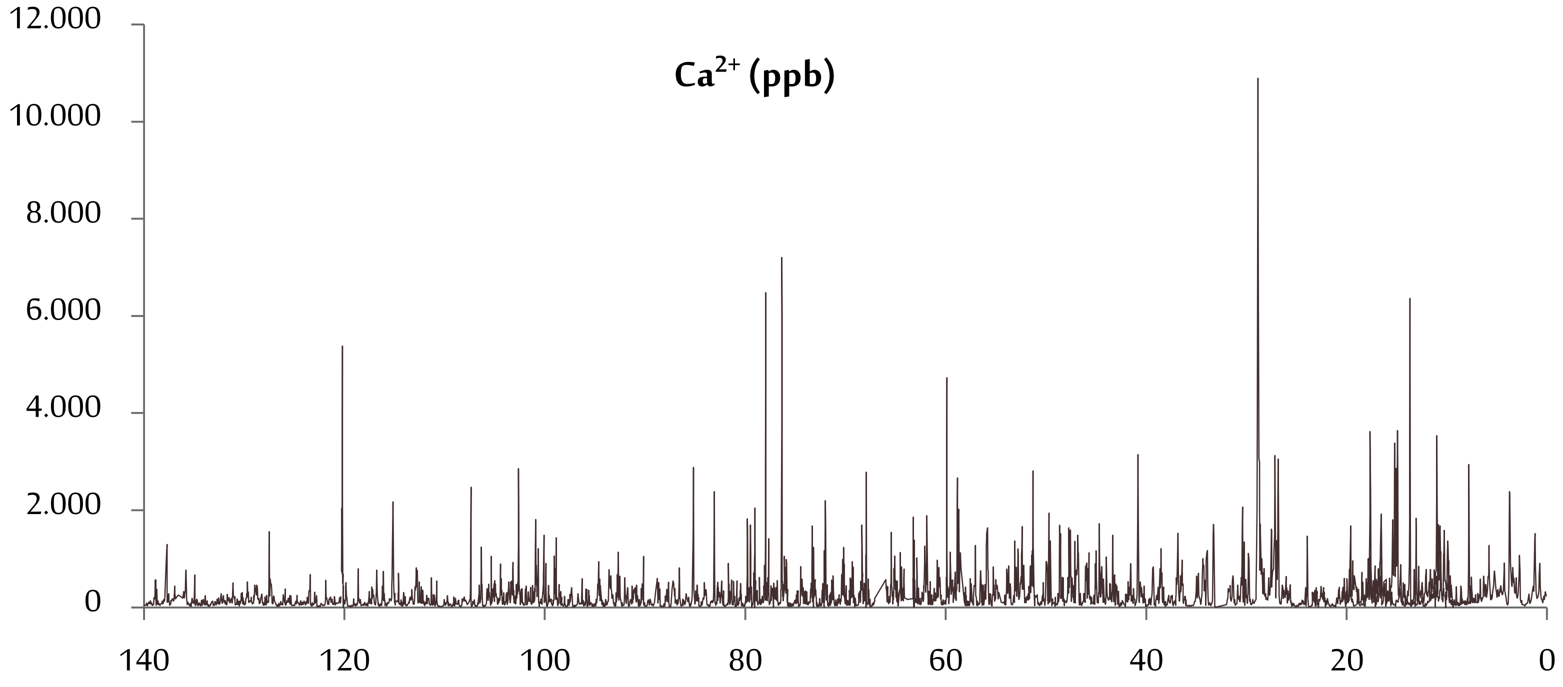
Ca2+ (ppb)
12.000
10.000
8.000
6.000
4.000
2.000
0
140
120
100
80
60
40
20
0

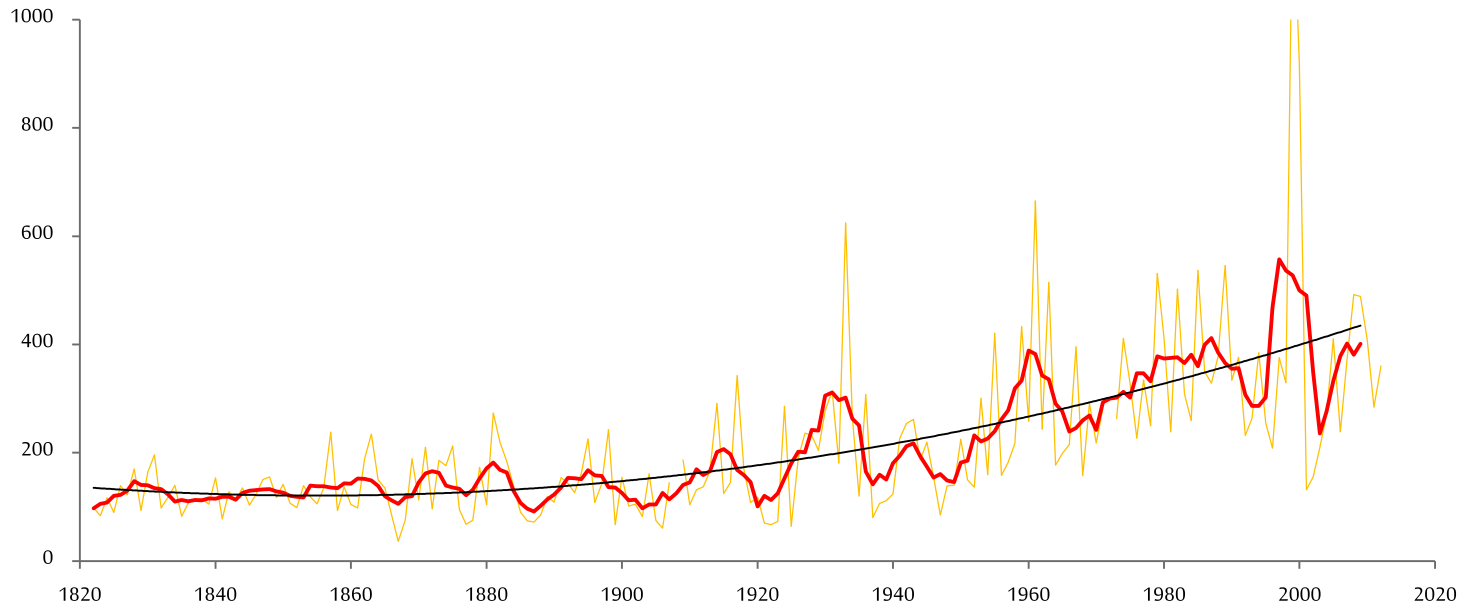
1000
800
600
400
200
0
1820
1840
1860
1880
1900
1920
1940
1960
1980
2000
2020

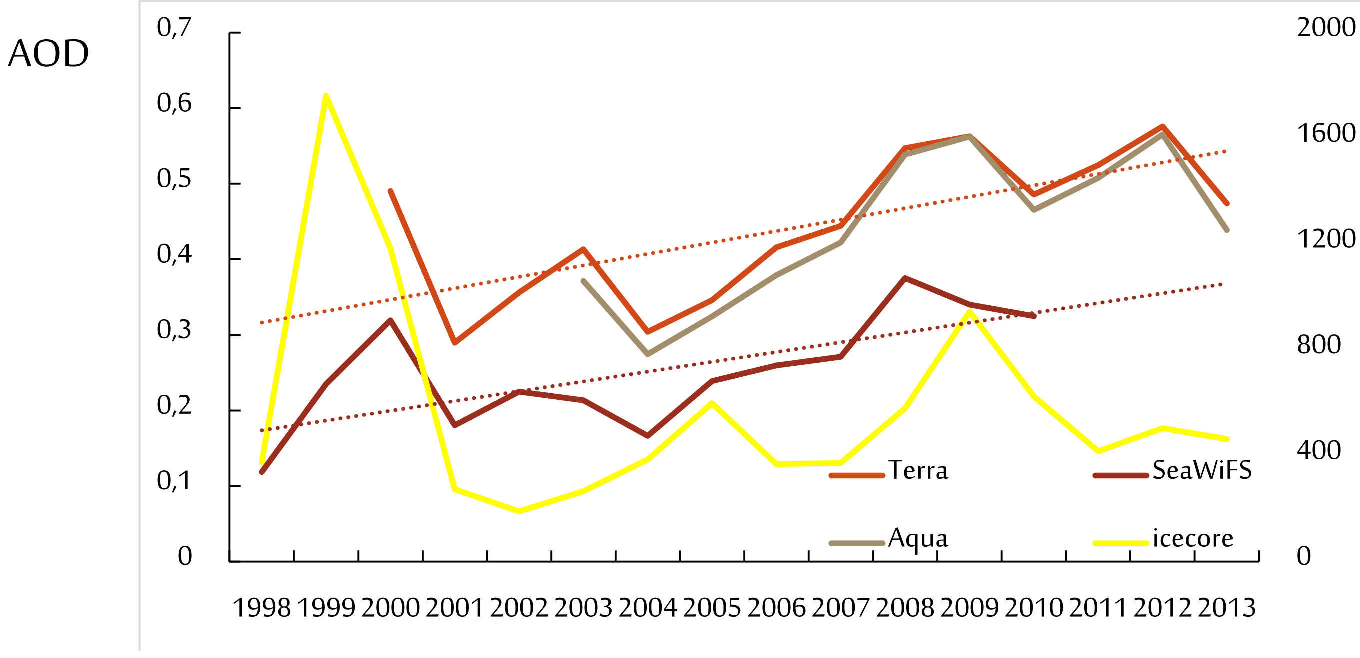

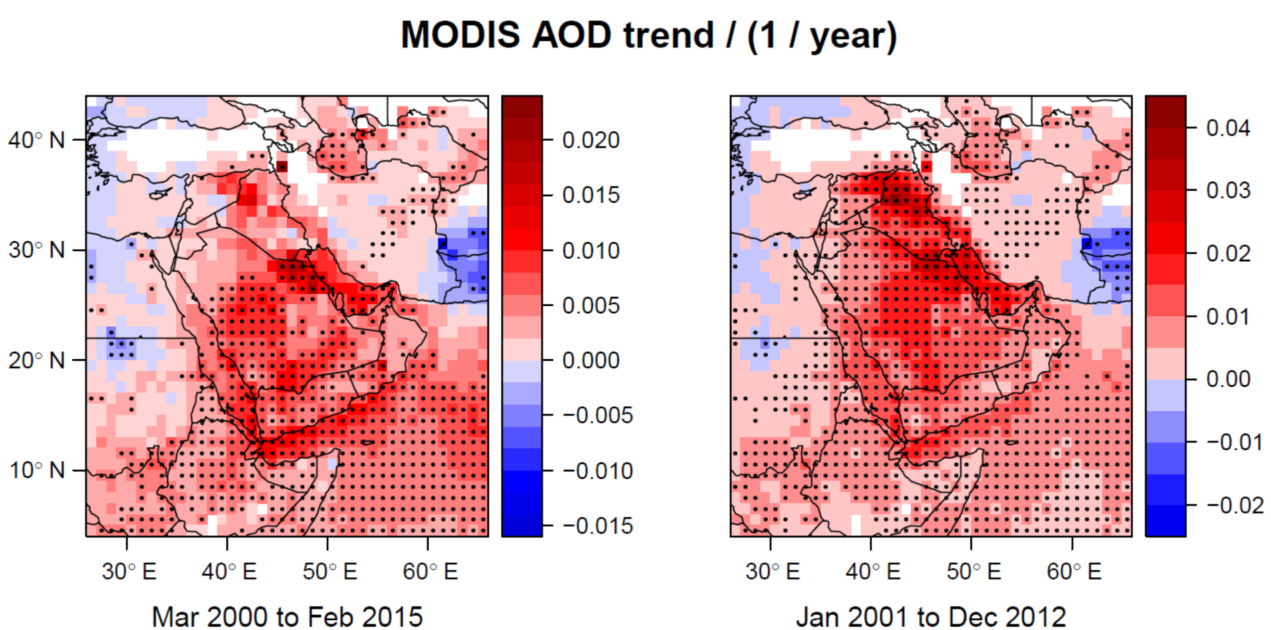

Klingmuller et al., 2016

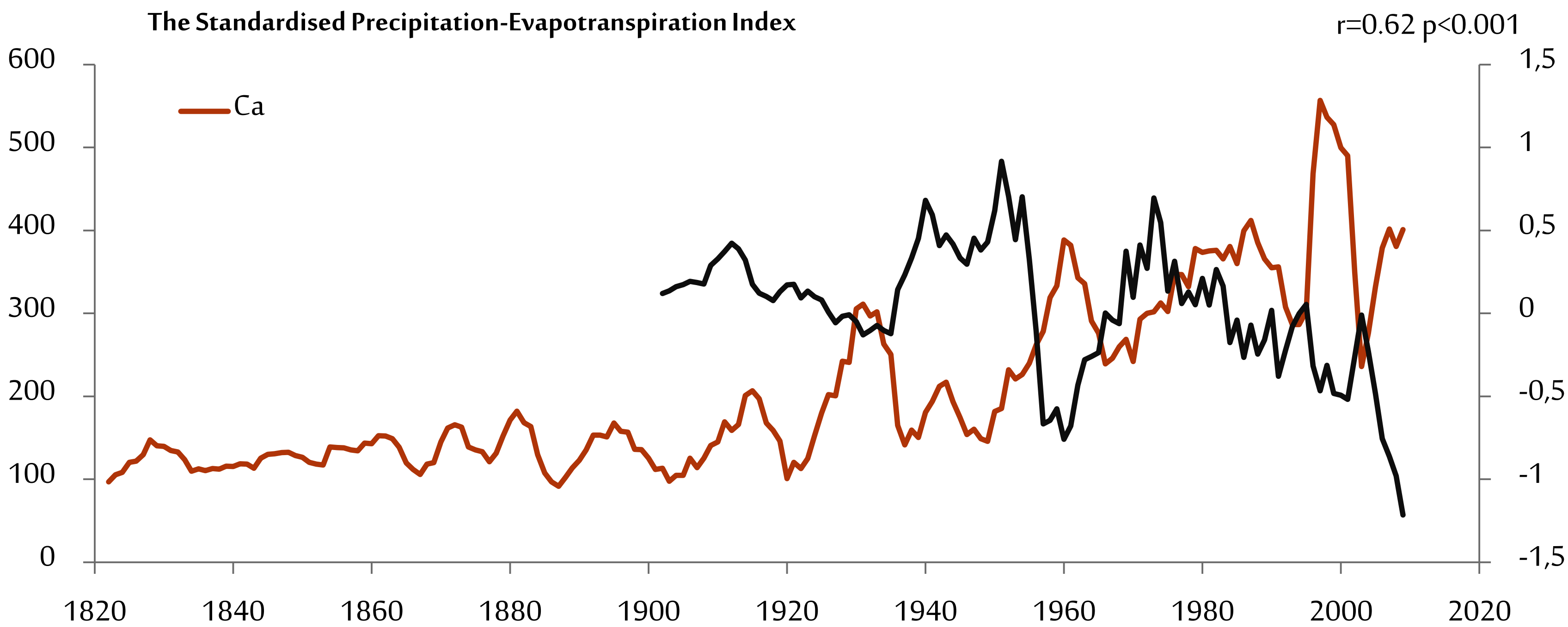
The Standardised Precipitation-Evapotranspiration Index
r=0.62 p<0.001
Ca
600
500
400
300
200
100
0
1,5
1
0,5
0
-0,5
-1
-1,5
1820
1840
1860
1880
1900
1920
1940
1960
1980
2000
2020

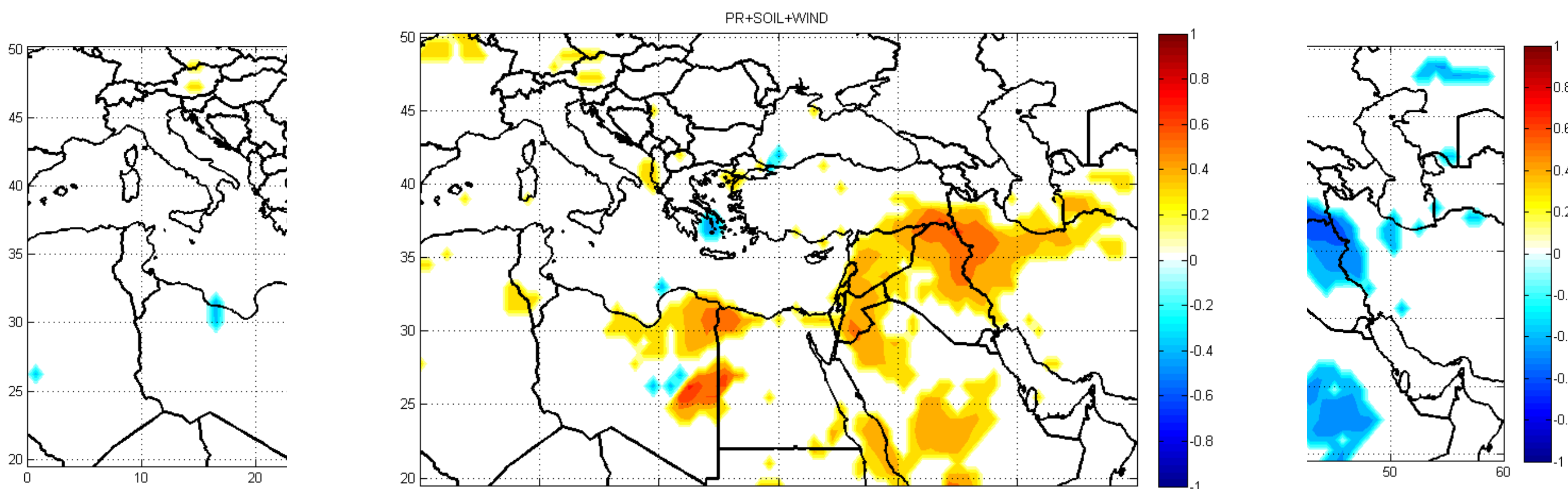
PR+SOIL+WIND

ELBRUS vs scPDSI from OWDA

(Cook et al., 2016)

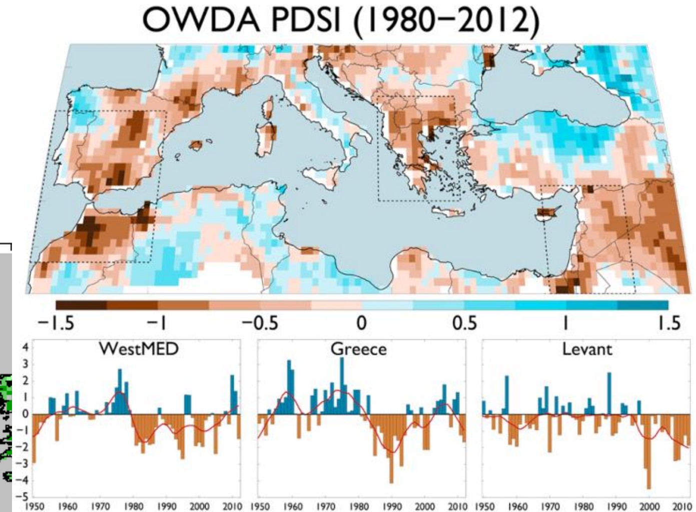

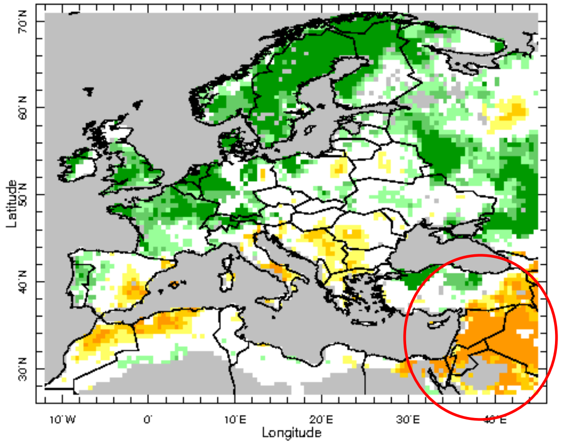

2000

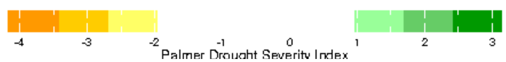

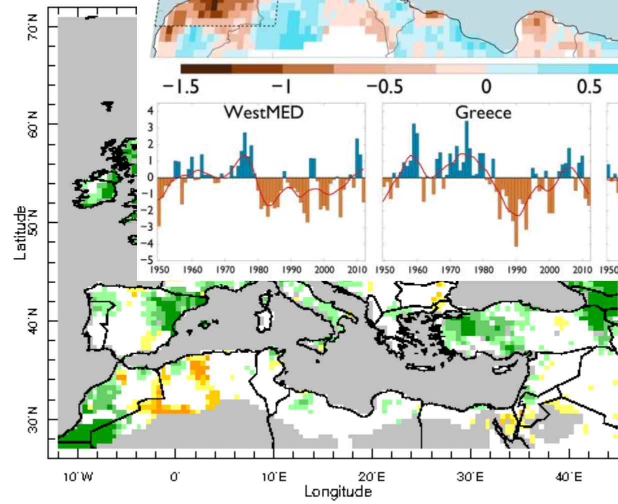

2002

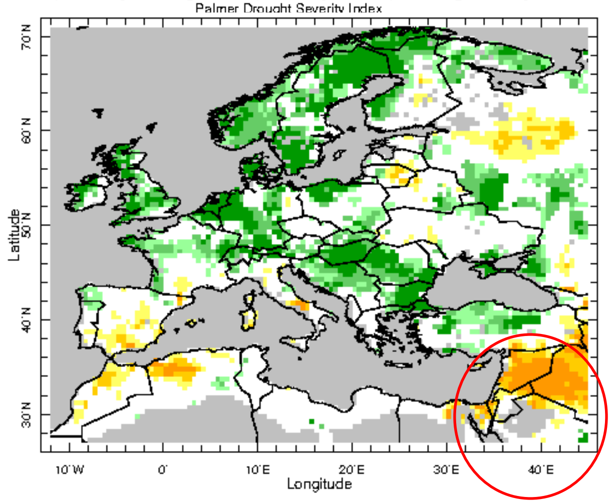

1999

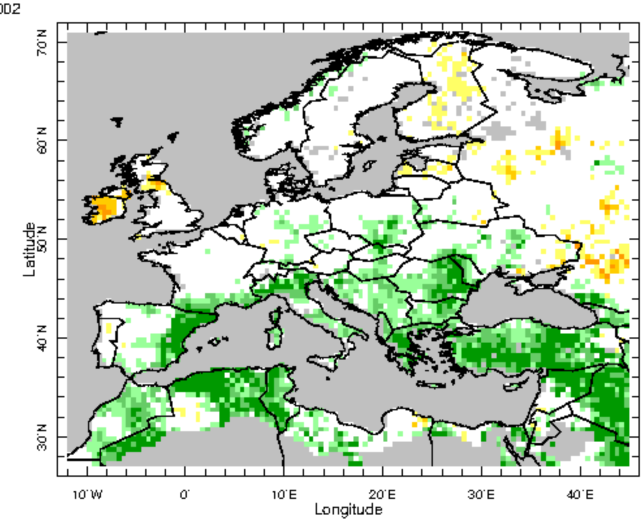

1972

"For the Levant we estimate that 1998–2012 in the OWDA is likely 89% likelihood) the **driest 15 year period** in the region since **the twelfth century**, with even greater confidence (98% likelihood) that it is **the driest back to 1500 C.E.**" (Cook et al., 2016)

The impact of the Pacific Decadal Oscillation on springtime dust activity in Syria

2016

Bing Pu[1,2] and Paul Ginoux[1,2]

	PDO	Niño 3.4	P1	P2	LAI1	LAI2	10 m wind
Aqua DOD	**−0.51**	**−0.24**	−0.05	−0.05	**−0.35**	**−0.41**	−0.00
Terra DOD	**−0.50**	**−0.23**	−0.05	−0.06	**−0.32**	**−0.39**	−0.02

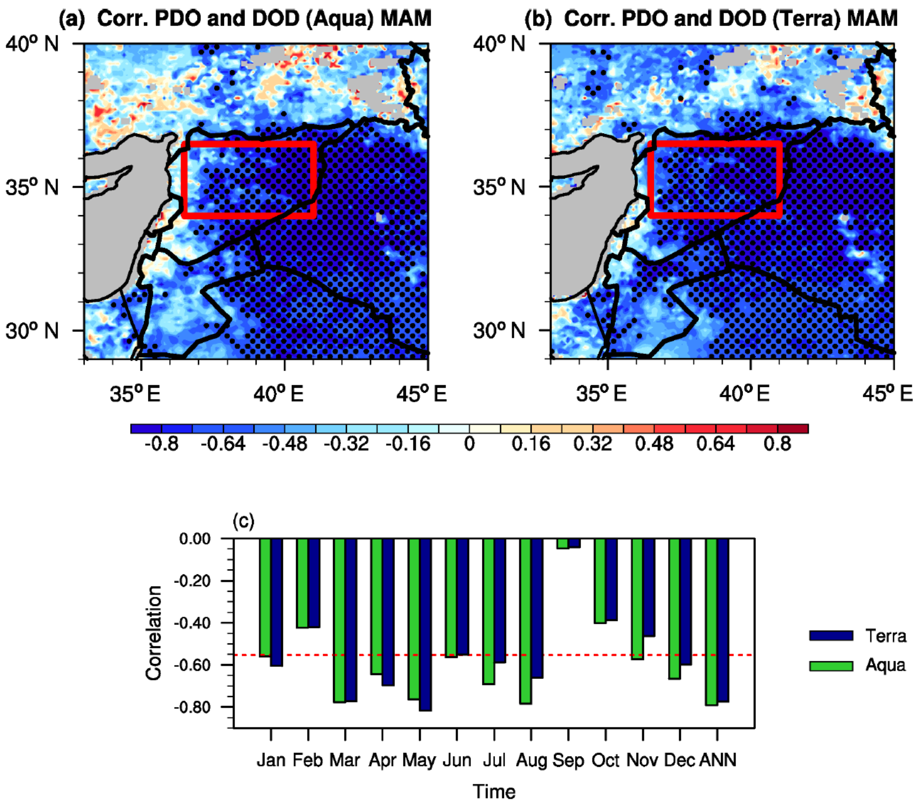

A significantly negative correlation is found between Syrian DOD and the PDO in springtime during 2003–2015, suggesting that the PDO index explains about 81% variances of Syrian DOD in spring in the recent decade.

The positive phase of the PDO tends to increase precipitation over the Arabian Peninsula and northeastern Africa.

A negative PDO thus is associated with wind and geopotential height patterns favorable to high DOD in Syria and also tends to reduce precipitation in the dust source regions such as Iraq, Saudi Arabia, and northeastern Africa

"The influences of the PDO on circulation and precipitation patterns over the Middle East largely persist beyond the recent decade, e.g., over 1948–2015, but also show some exceptions. The lack of long-term observations also brings uncertainties to the connection between the PDO and Syrian DOD."

PDO

corr Jan−Dec averaged Ca Summer index
with Jan−Dec averaged HadISST1 SST 1980:2000 p<10%

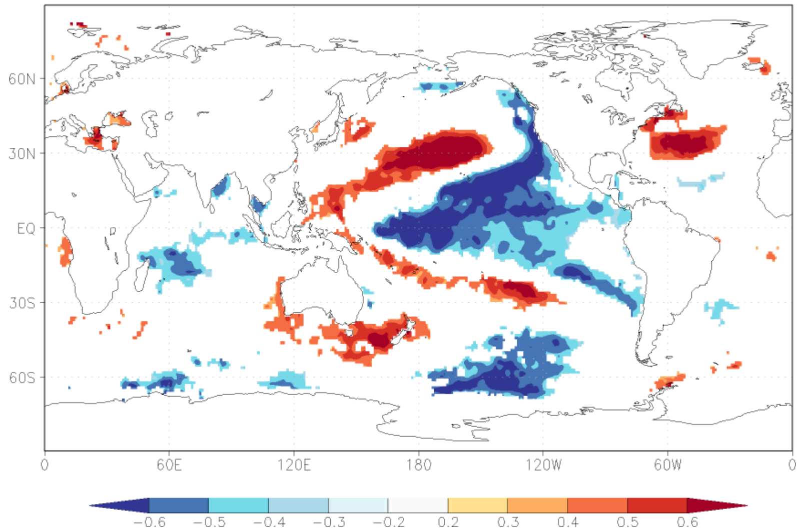

corr Mar−May averaged Ca Summer index
with Mar−May averaged HadISST1 SST 1980:2008 p<10%

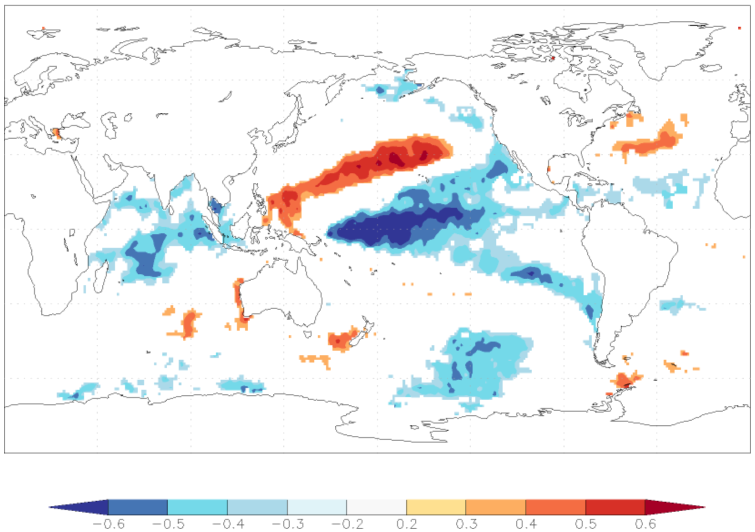

corr Mar−May averaged Ca Summer index
with Mar−May averaged HadISST1 SST 1950:2008 p<10%

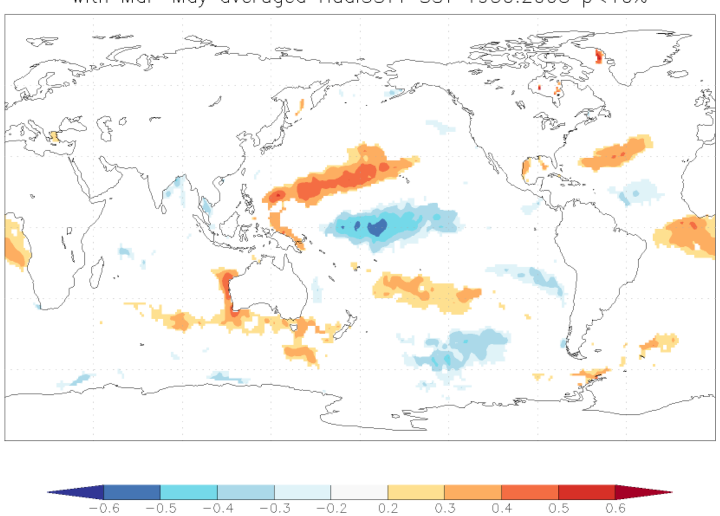

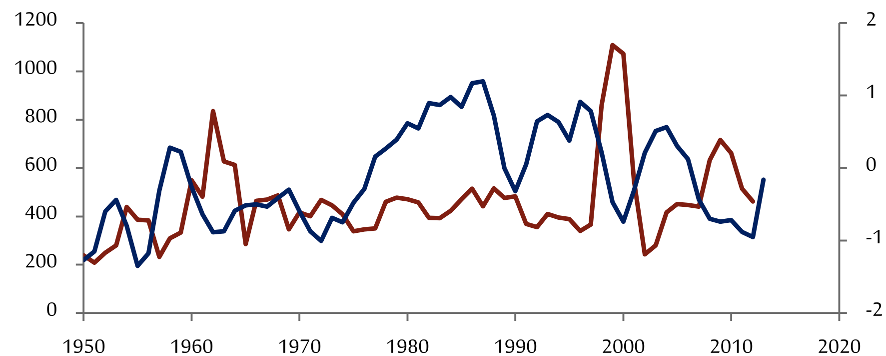

Summary

- ✓ Elbrus ice core is the first ice core to represent environmental changes in the Middle East region
- ✓ Frequent dust events affect Caucasus glaciers in Spring-Summer
- ✓ Variations in Ca^{2+} concentration are related to the drought conditions in Syria-Iraq region
- ✓ There is a prominent increase in distant dust concentration in the ice core over the past 200 years

-Mechanisms responsible for dust variations are yet to be understood.

Ongoing work

- distinction between Sahara and Middle East events
- more strict separation of individual dust events, frequency analysis and comparison to background concentrations
- mineralogical analysis
- comparison to observations and proxy data
- better understanding of changes in circulation
- combined analysis of NH_4, SO_4 and dust
- longer record

- RSF grant 17-17-01270
- European Union Seventh Framework Programme FP7-PEOPLE-2010-IIF under grant agreement PIIF-GA-2010-275071,
- Russian Foundation for Basic Research (grants 11-05-00304 and 13-05-10069).

References: [Kutuzov et al. 2013; Shahgedanova et al. 2013; Mikhalenko et al., 2015; Kutuzov et al., 2016]